Chapter 1

Introduction and Objective

1.1 Introduction

This project aims at improving the efficiency of most commonly used centrifugal pumps. These pumps have a wide area of applications in households, industries and irrigation. The efficiency of majority of these pumps is very low and hence a large amount of input energy is going waste. One can easily recognize that huge amount of energy savings can be made through better design and control of pump systems, given the large number of pumps in the field. The approach requires proper expertise to identify the best solution in terms of impeller design (Hydrodynamic) as well as motor selection (Power Requirements).

A centrifugal pump works by the conversion of the rotational kinetic energy, from an electric motor, to an increased static fluid pressure. The rotation of the pump impeller imparts kinetic energy to the fluid as it is drawn from the impeller eye and is forced out through the impeller vanes. As the fluid exits the impeller, fluid kinetic energy is converted into static pressure due to change in area of the volute section.

A survey conducted by Gupta & Goel [1] clearly bought out the fact that the pumps of 1 HP or higher ratings have efficiency higher than 60%. It is also showed that whenever 3 phase motors are used, the efficiencies are better than the pump of similar head and running capacity on single phase motors.

Based on the previous work done, a Crompton Greaves pump (Model No. MBE052, 0.5HP single phase), with measured best overall efficiency of 26.56% was considered for the efficiency improvement.

In the first phase of the work, results of Gupta & Goel [1] are reproduced. This was done by experimental verification of their obtained efficiency values followed by re-run of their FLUENT simulations. It was found out that performance of the pump reassembled was significantly lower than before disassembly. As such a new pump of same specification was purchased and all the efficiency measurement tests were repeated.

After the completion of testing on new pump, the old pump was disassembled and the impeller and the casing were taken out for blade profile measurements. A Coordinate Measuring Machine (CMM) was used to measure physical geometrical characteristics of the impeller and the casing. Using these measured characteristics, CAD model was made using SOLID WORKS and subsequently used for CFD analysis in FLUENT and GAMBIT and Stress Analysis in ANSYS.

CFD technique is applied to predict whether velocity profiles in the mid path of flow area is along the blade profile or not. The flow field through the impeller is analyzed to investigate the effect of change in flow area on the pressure developed in the flow. Various modified impeller designs are presented by varying flow area.

1.2 Objectives

The specific objectives of this project are: -

1. To identify a less efficient water pump (based on the previous work done by Gupta & Goel [1]) and verify it's experimentally obtained performance characteristics.

2. Re-design the pump impeller for increasing the efficiency and evaluate it using CFD analysis.

3. Stress analysis of improved impeller using ANSYS and material selection.

4. To fabricate the re-designed impellers and test their performance.

5. Select an electric motor with higher efficiency to operate the pump.

6. Test and demonstrate the improved motor-pump system.

1.3 Organization of the Report

The report begins with the introduction to this project in chapter 1, followed by the work plan, the methodology and the literature review in chapter 2. It also contains a brief introduction to various simulation softwares used and scope of the present work. Chapter 3 and chapter 4 are exclusively dedicated to work done in the project. While chapter 3 covers all the experimental work, all simulation results are given in chapter 4.

In chapter 5 we have discussed our various results and scope of future work.

Chapter 2

Literature Review and Work Plan

2.1 Radial Flow Pumps

These pumps are often referred to as just centrifugal pumps. The fluid enters along the axial plane, is accelerated by the impeller and exits at right angles to the shaft (radially). These operate at higher pressures and lower flow rates than axial and mixed flow pumps.

2.2 Basics of Centrifugal Pumps

A centrifugal pump is one of the simplest pieces of equipment in any process plant. Its purpose is to convert the energy of prime mover (Electric Motor) first into velocity (Kinetic Energy) and then into pressure energy of fluid that is being pumped. The energy changes occur by the virtue of two main parts of the pump, the impeller and the volute or the diffuser. The impeller is the rotating part that converts driver energy into kinetic energy. The volute or diffuser is the stationary part that converts the kinetic energy into pressure energy.

Generation of Centrifugal Force

The process liquid (generally water) enters the suction nozzle and then into the eye of a revolving device known as impeller. When the impeller rotates, it spins the liquid sitting in the cavities between the vanes outward and provides centrifugal acceleration. As the liquid leaves the eye of the impeller, a low pressure area is created causing more liquid to flow towards the inlet. Because the impeller blades are curved, the fluid is pushed in a tangential and radial direction by the centrifugal force.

Conversion of Kinetic Energy to Potential Energy

The amount of energy given to the liquid is proportional to the velocity at the edge or vane tip of the impeller. The faster the impeller revolves or bigger the impeller is, the higher will be the velocity of the liquid at the vane tip and greater the energy imparted to the liquid. The kinetic energy of the liquid is harnessed by creating a resistance to the flow. The first resistance is created by the pump volute (Casing) that catches the liquid and slows it down. In the discharge nozzle, the liquid further decelerates and its velocity is converted into pressure according to Bernoulli's principle [2].

2.3 Definition of Important Terms

The key performance parameters of centrifugal pumps are Capacity, Head, Brake Horse Power (BHP), Best Efficiency Point (BEP) and Specific Speed. The pump curves provide the operating window within these parameters can be varied for satisfactory pump operation [3]. The following parameters are discussed in detail in this section.

i) **Capacity (Q)**: It is the flow rate with which liquid is moved or pushed by the pump to the desired point in the process. It depends on the number of factors such as liquid characteristics (Viscosity and Density), size of pump (inlet and outlet sections) size and rotational speed of impeller, pump suction and discharge temperatures and pressure conditions.

ii) **Head (H)**: It indicates pressure caused by a liquid due to its weight. It is significantly different from pressure developed by a pump. If specific gravity of liquid changes than pressure developed by a pump will change but head developed will remain constant.

iii) **Input Power (P_{in})**: It is actual power delivered to the shaft.

iv) **Hydraulic Power Output (P_{out})**: It is the power delivered to the liquid by the pump.

$$P_{out} = \rho QgH$$

v) **Pump Efficiency (η_o)**:

$$\eta_o = \text{Power Input/ Power Output}$$

$$= \rho QgH/P_{in}$$

vi) **Best Efficiency Point (BEP)**: It is the capacity at which the efficiency is highest. All points to the right or left of BEP have a lower efficiency. It is the measure of optimum energy conversion. When sizing and selecting centrifugal pumps for a given application the pump efficiency at design should be taken into consideration. The efficiency represents a unit of measure describing the change of centrifugal force (expressed as velocity of fluid) into the pressure energy. Given that the pump is running at a give speed, vary the flow rate in the whole range of the pump and measure the corresponding head. The power output is calculated by the total differential head multiplied by the flow rate and the power input to the motor is directly measured. The ratio of P_{out} to P_{in} is calculated at different points and the point at which this ratio is highest is the BEP. It is generally preferred that pumps operate within 80% to 110% of BEP for optimum performance [7].

vii) **Specific Speed (N_s)**: It is a non-dimensional number used to classify pump impellers as to their type and proportions. It is defined as the speed in revolutions per minute at which a geometrical similar impeller would operate if it were of such a size as to deliver one gallon per minute against one foot of head [4]. Pumps of same specific speed but different size are considered to be geometrically similar, one pump being size-factor of the other.

$$Ns = N*Q^{(1/2)}/H^{(3/4)}$$

As the specific speed increases, the ratio of the impeller outlet diameter to the inlet or eye diameter decreases. The ratio becomes 1 for a true axial flow impeller. Low specific speed radial flow impellers develop head principally through centrifugal force. Pumps of higher specific speed develop head partly by centrifugal force and partly by axial force. An axial pump or a propeller pump with a specific speed of 10,000 or greater generates its head exclusively through axial forces. Radial impellers are generally high head/low flow designs [4].

Typical recommended range of specific speed for different types of pumps is as follows [7]: -

- Radial Flow – $9.76<N_s<78.06$; N in RPM, Q in m^3/s, H in m.
- Mixed Flow – $39.03<N_s<156.12$; N in RPM, Q in m^3/s, H in m.
- Axial Flow – $136.50<N_s<390$; N in RPM, Q in m^3/s, H in m.

viii) **Net Positive Suction Head (NPSH)**: - It is the total head at the suction flange of the pump less the vapor pressure converted to fluid column height of liquid. As the liquid passes from the pump suction to the eye of the impeller, the velocity increases and pressure decreases. There are also pressure losses due to shock and turbulence as the liquid strikes the impeller. The centrifugal force of the impeller vanes further increases the velocity and decreases the pressure of the liquid. The NPSH required is the positive head required at the pump suction to overcome these pressure drops in the pump and maintain the majority of liquid above its vapor pressure. The NPSH required varies with the speed and capacity within any particular pump. It increases as the capacity is increasing because the velocity of the liquid is increasing, and as anytime the velocity of a liquid goes up, the pressure or head comes down. The NPSH is independent of density of the fluid.

2.4 Affinity Laws

The affinity laws are mathematical expressions that define changes in pump capacity, head and BHP when a change is made in the pump speed, impeller diameter, or both.

i) Capacity (Q) changes in direct proportion to impeller diameter D ratio, or to speed N ratio:

$$Q_2 = Q_1*[D_2/D_1]$$

$$Q_2 = Q_1*[N_2/N_1]$$

ii) Head (H) changes in direct proportion to the square of impeller diameter D ratio, or to square of speed N ratio:

$$H_2 = H_1*[D_2/D_1]^2$$

$$H_2 = H_1*[N_2/N_1]^2$$

iii) BHP changes in direct proportion to the cube of the impeller diameter ratio, or the cube of the speed ratio:

$$BHP_2 = BHP_1*[D_2/D_1]^3$$

$$BHP_2 = BHP_1*[N_2/N_1]^3$$

2.5 Pump and Motor Testing Standards

Pump Testing: Experimental setup was designed as per Indian Standard Centrifugal, Mixed Flow and Axial Flow Pumps- code for Hydraulic Performance tests- Precision Class (IS 13538:1993) [2]. Pump testing is used for measurement of flow rates, speed of rotation, power input and calculation of pump efficiency. Details of the procedure are presented in Chapter 3.

Motor Testing: The equivalent circuit parameters for a motor can be determined using specific tests on the motor. These are in accordance with Indian Standard 7572: Guide for testing Single Phase and universal motors [3].

i) **No-Load Test**: - Balanced voltages are applied to the stator terminals at the rated frequency with the rotor uncoupled from any mechanical load. Current, voltage and power are measured at the rotor input. The losses in the no-load test are those due to core losses, winding losses, windage and friction. Given that the rotor current is negligible under no-load conditions, the rotor copper losses are losses are also negligible. Thus, the input power measured in the no-load test is equal to the stator copper losses plus the rotational losses.

$$P_{NL} = P_{Cu1} + P_{rot}$$

Where the stator copper losses are given by

$$P_{Cu1} = I^2_{NL}*R_{w1}$$

From the no-load measurement data (V_{NL}, I_{NL}, P_{NL}), the value of R_{NL} is determined from the no-load dissipated power.

ii) **Blocked Rotor Test**: - The rotor is blocked to prevent rotation and balanced voltages are applied to the stator terminals so that the rated current is achieved. Current, voltage and power are measured at the motor input. In this case the speed dependent resistance goes to zero and thus rotational losses go to zero. Thus we can get value of copper losses (P_{Cu1}).

2.6 Material Properties

Material selection for the impeller is also important both structurally as well as in terms of inertness with the working fluid. In our case, the working fluid is water. Hence the important criterion that comes into effect is that material should be able to handle various stresses generated due to rotation of impeller and due to fluid pressure.

Another criterion is the surface roughness of the impeller. The existing impeller is made of Cast Iron and has a very high surface roughness. This would result in turbulence in flow through impeller and would bring down its efficiency.

2.7 Computational Fluid Dynamics

CFD (Computational Fluid Dynamics) is one of the branches of fluid mechanics that uses numerical methods and algorithms to solve and analyze problems that involve fluid flows. Computers are used to perform the millions of calculations required to simulate the interaction of liquids and gases with surfaces defined by boundary conditions [5].

In all of the CFD problems, the same basic procedure is followed:-

i) The geometry (physical boundary) of the problem is defined.
ii) The volume occupied by the fluid is divided into discrete shells (mesh). This division may be uniform or non-uniform.
iii) The physical model is defined – for example, the equations of motion + enthalpy + species conservation.
iv) Boundary conditions are defined. This involves specifying the fluid behavior and the properties at the boundaries of the problem. For transient boundary conditions initial conditions are also identified.
v) The set of above equations identified above are discretized over the mesh and solved numerically on computer.
vi) Finally a postprocessor is used for the analysis and visualization of resulting solution.

2.8 Computational Software for CFD and FE analysis

i) **ANSYS**: It is a general purpose finite element modeling package for numerically solving a wide variety of mechanical problems. These problems include static/dynamic structural analysis (both linear and non-linear). The steps to be followed are similar to the ones in CFD. Meshing is done after defining geometrical properties on which structural analysis is done.

ii) **Gambit & Fluent**: Fluent is a general purpose CFD code based on the finite volume method. This technology offers a wide array of physical models for applying to wide variety of problems. Gambit is a geometric modeling and grid generation tool often used with Fluent Technology. It allows users to create their own geometry or import geometry from most of the CAD packages.

2.9 Rapid Prototyping

It is the automatic construction of physical objects using additive manufacturing technology. The use of additive manufacturing technology for rapid prototyping takes virtual design from Computer Aided Design (CAD), transforms them into thin, virtual, horizontal cross sections and then creates successive layers until the model is complete. Through this process the virtual model and the physical model created are almost identical [2].

2.10 Work Plan

Our main work elements are listed below:-

i) Literature Review.
ii) Experimental validation of previous work by pump testing and motor testing.
iii) CFD analysis of existing pump and its comparison with the previous work.
iv) Re-design of impeller blades by varying its geometric features and estimation of its efficiency using CFD simulation.
v) Stress analysis of re-designed impeller using ANSYS and selection of suitable material for fabrication.
vi) Fabrication of the impeller.
vii) Testing of the fabricated impeller for its estimated efficiency.
viii) Coupling the new motor pump system and testing for performance.

2.11 Scope of Present Work

The work done in the project started with the literature review about the basics of centrifugal pumps covering their functioning and applications. Special emphasis is laid on Pump and Motor testing standards since a major part of the work involved experiments to calculate the efficiency of Pump and Motor. The other work that was done simultaneously with the other things was learning of software Solid Works for CAD Modeling, Fluent & Gambit for CFD and ANSYS for FE analysis. After the literature review, experimental results of Gupta & Goel [1] are verified for Crompton Greaves Pump (Model No. MBE052). For these experiments experimental rig was set up as per Indian Standards of Pump and Motor Testing. Since Gupta & Goel [1] had disassembled the pump, a new pump was purchased to verify various performance parameters of the pump. After carrying out the experiments, old pump was disassembled and the impeller and the casing were separated, taken out and all the dimensional measurements were done using CMM (Coordinate Measuring Machine). Using these measurements, CAD models of impellers and casing were created which were subsequently used for Flow modeling in Gambit & Fluent and FE analysis in ANSYS.

In order to test modified impellers it was decided that RPT facility can be used. As such existing impeller was also fabricated using RPT method and was used in the dissembled old pump. A comparison is shown between all the results obtained using Cast Iron impeller and RPT impeller.

During last part of the work various modified impeller geometries are presented and their performance is evaluated using CFD analysis.

2.12 GANTT CHART

BTP Part 1

Week/Work	1	2	3	4	5	6	7	8	9	10	11	12	13	14
Literature review														
Experimentation														
CFD analysis of existing pump														
Redesign of pump														
CFD simulation of redesigned pump														
Stress Analysis on ANSYS														

BTP Part 2

Week/Work	1	2	3	4	5	6	7	8	9	10	11	12	13	14
Matrial Identification														
Fabrication of impeller prototype														
Testing of impeller														
Electric motor selection														
Testing of improved motor pump system														
Eventualities														

Chapter 3

Experimental Work

We have presented our experiment work under various sections. Section 3.1 deals with experiments carried out with old Crompton Greaves Pump. This also includes a comparison with results obtained by Gupta & Goel [1]. A detailed explanation is given for experimental procedure for Pump and motor testing as per Indian Standards. Section 3.2 covers experiments carried out with new pump of the same configuration followed again by comparative analysis.

Results of experiments carried out using RPT impeller are given in Section 3.3. During experimentation it was observed that there is some lateral movement of the impeller on the motor shaft. It was rectified by using a steel washer. Later another RPT impeller was fabricated without above anomalies. Experimental results of RPT II impeller are discussed in Section 3.4.

3.1 Experiments on Old Crompton Greaves Pump

3.1.1 Experiment 1

IS Standards (IS 13538-1993) [2]: This standard specifies measurement of flow rate either by "Static Weighing Method" or by "Dynamic Weighing Method". In our experimentation we have preferred to use the "Dynamic Weighing Method" where the weighing is made "in flight", the flow being directed permanently into the tank.

The weighing method, which gives only the value of the average flow rate during the time taken to fill the weighing tank, may be considered the most accurate method of flow rate measurement.

It should also be noted down that the weighing method require large fixed installations which are only practicable in a laboratory and for relatively less flow rates ($<1.5\ m^3/s$).

Depending on the installation conditions of the pump and on the layout of the circuit, the pump head may be determined either by measuring the inlet and outlet total heads separately, or by measuring the differential pressure between inlet and outlet and adding the differences in velocity head, if applicable taking into account potential head and density variations due to the measuring system.

Pump testing: - The old testing rig had been dismantled so a new test rig was setup as per the Indian Standards [2], as shown in Figure 3.1. The flow rate was controlled by a gate valve at the outlet. The discharge pressure was measured using a pressure gauge and suction pressure using a mercury U-tube manometer (30^{o} inclination) which is open at one end to the atmosphere. The flow rate was measured using a gravimetric tank where the time is noted for 50 kg (20 kg in some of the experiments; Mentioned where used) increase in mass of water in the tank. The input current, voltage and power were measured across the terminals of the motor. Table 3.1 shows the efficiency calculations for the Crompton Greaves pump MBE052. It is seen that the peak efficiency is 17.87% at a flow rate of 1.66 L/s. This is the design point for this pump (BEP).

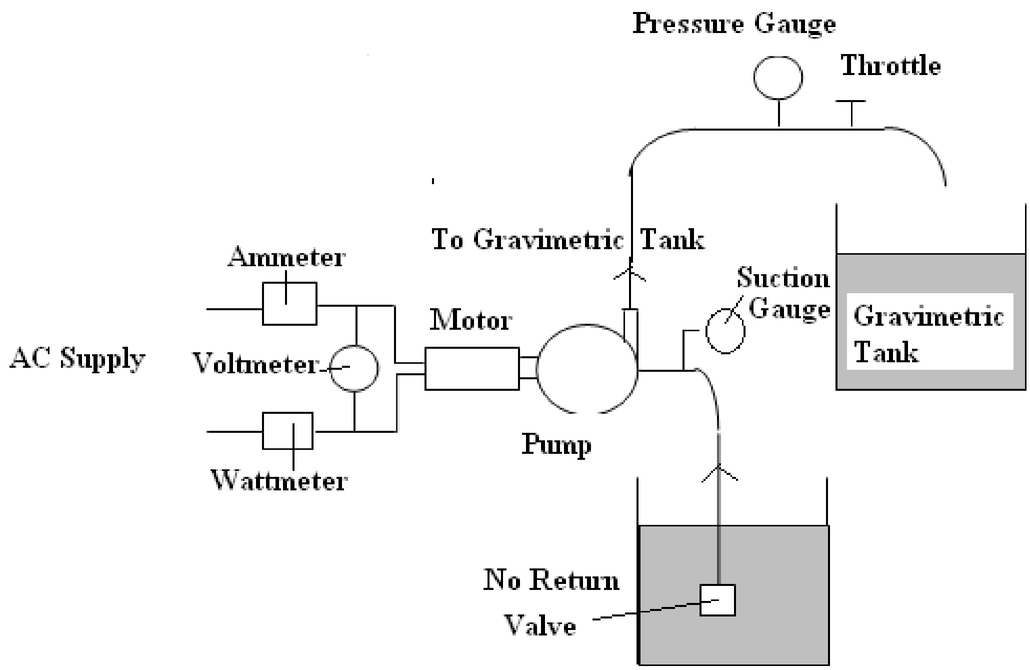

Figure 3.1 Experimental Setup for Pump Performance Testing as per IS-13538:1993 [2]

Motor test: - The setup includes a variable voltage transformer to supply variable voltage to the motor, a voltmeter, an ammeter and a wattmeter.

No-Load Test: - The rotor is uncoupled from any mechanical load and balanced voltages are applied to the terminals. The rotational losses in the no-load test are due to core losses, winding losses and friction. Measure values of voltage, current and power are shown in Table 3.2.

Table 3.1 Efficiency Calculations for old Crompton Greaves Pump-Experiment 1

Discharge Pressure (gauge)	Suction Pressure		Input Power (P_{in})	Flow rate (Q)	Efficiency (η_o)
(atm)	Suction Side (cm)	Open to atm. (cm)	(Watts)	(L/s)	(%)
0.177	77.7	20	1049.5	1.981	12.09
0.354	76.9	20.75	1047.3	1.902	14.61
0.531	75	22.6	1039.5	1.786	16.37
0.708	73.1	24.25	1024	1.661	17.87
0.885	69.35	27.45	988.85	1.407	17.39
1.062	66.35	30.3	946.2	1.076	15.36
1.180	63.5	32.5	903.4	0.849	13.44

Table 3.2 Readings from No-Load test of the Motor

S.No	Rated Voltage (V)	Current (A), I_{NL}	Input Power (W), P_{NL}
1	200	2.3	265.2

Blocked Rotor Test: The rotor is blocked to prevent its rotation. The voltage is applied to the stator terminals such that the rated current is achieved. Current, voltage and power are measured at the motor input and are shown in Table 3.3.

Table 3.3 Readings from Block Rotor test of the motor

S.No	Voltage (V_{BR})	Rated Current (A), I_{BR}	Input Power (W), P_{BR}
1	56.9	4.0	197.2

Sample calculation

The copper losses and the rotational losses are calculated from these data.

Copper losses = I_{BR}^2R = 197.2 W.

Rotational losses = $P_{NL} - 2.30^2R$ = 200W.

Therefore the total losses = 397.2W

The rotational losses remains constant and the copper losses vary with the current in each case with the flow rate. Based on these motor losses, the motor efficiency can be calculated for various cases. Since the overall efficiency was determined from the experiments, the pump efficiency can be found out. Efficiency values are calculated for set of observations as shown in Table 3.4.

For this pump the overall best efficiency is17.87%, the power delivered to the discharge fluid is 183.02W; motor efficiency is 44.06% thereby giving a pump efficiency of 40.56%.

The pump efficiency obtained was much lower as compared to 50.94% mentioned in the previous report by Gupta and Goel [1]. The possible losses could be due to leakage, improper sealing, high friction inside impeller due to heavy rusting, improper shaft lubrication. The voltage obtained from the AC source during the course of the experiment is recorded at 200V which is low as compared to 220V that is generally obtained. This can also be a source of increase in input power to the motor. The motor efficiency also has come down to 44.06% as compared to 52.14% as in [1]. This was accounted to increase in resistance as evident from the calculations. In order to sort out the significant losses, it was decided to carry out the experiment once again with sufficient care taken in lubrication, efficient sealing, and reduction of impeller rustiness and at 220V AC source. The impeller was soaked in diesel for a whole day to get rid of the rustiness as shown in Figure 3.2.

Table 3.4 Efficiency Calculations for the Motor and the Impeller-Experiment 1

Input Power (P_{in}) (Watts)	**Output Power (P_{out}) (Watts)**	**Overall Efficiency (η_o) (%)**	**Input Current (I) (Amperes)**	**Motor Power Loss (Watts)**	**Pump Input Power (P_{pump}) (Watts)**	**Motor Efficiency (η_{motor}) (%)**	**Pump Efficiency (η_{pump}) (%)**
1049.5	126.877	12.09	5.6	586.512	462.988	44.115	27.404
1047.25	153.032	14.61	5.6	586.512	460.738	43.995	33.215
1039.5	170.146	16.37	5.5	572.83125	466.66875	44.894	36.460
1024	**183.015**	**17.87**	**5.5**	**572.83125**	**451.16875**	**44.059**	**40.565**
988.85	172.008	17.39	5.4	559.397	429.453	43.430	40.053
946.2	145.345	15.36	5.4	559.397	386.803	40.880	37.576
903.4	121.394	13.44	5.4	559.397	344.003	38.079	35.289

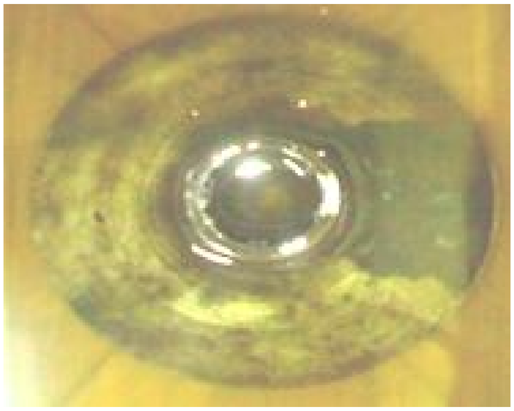

Figure 3.2 Impeller soaked in diesel to remove the rust

3.1.2 Experiment 2

The experiment is repeated again using the cleaned impeller and a healthy functioning foot valve to prevent any leakage. The procedure carried out is the same as stated for the Experiment 1 and as per the Indian Standards [2]. The various experimental results (Efficiency and Flow rates) obtained are tabulated and shown below in Table 3.5:

Table 3.5 Efficiency Calculations for old Crompton Greaves Pump-Experiment 2

Discharge Pressure (gauge)	**Suction Pressure**		**Input Power (P_{in})**	**Flow rate (Q)**	**Efficiency (η_o)**
(atm)	**Suction Side (cm)**	**Open to atm. (cm)**	**(Watts)**	**(L/s)**	**(%)**
0.177059	72.6	24.3	864	1.997	13.39
0.354118	71.2	25.8	848	1.916	16.59
0.531178	69.2	27.6	836	1.776	18.71
0.708237	67.8	29.1	822	1.647	20.72
0.885296	65.2	31.5	797	1.452	21.33
1.062355	**62.8**	**33.4**	**764**	**1.292**	**22.23**
1.239415	57.6	37.8	711	0.842	16.76

As evident from the above table, the overall efficiency has increased to 22.23% at the BEP. The input AC voltage was recorded at 220V. The input power to the pump also reduced as compared to the Experiment 1.

The corresponding motor and the pump efficiencies were also calculated and are shown in a tabular form in Table 3.6.

Table 3.6 Efficiency Calculations for the Motor and the Impeller-Experiment 2

Input Power (P_{in}) (Watts)	**Output Power (P_{out}) (Watts)**	**Overall Efficiency (η_o) (%)**	**Input Current (I) (Amperes)**	**Motor Power Loss (Watts)**	**Pump Input Power (P_{pump}) (Watts)**	**Motor Efficiency (η_{motor}) (%)**	**Pump Efficiency (η_{pump}) (%)**
864	115.647	13.385	4.6	460.797	403.203	46.667	28.682
848	140.667	16.588	4.71	473.419	374.581	44.172	37.553
836	156.377	18.705	4.56	456.281	379.719	45.421	41.182
822	170.290	20.717	4.47	446.265	375.735	45.710	45.322
797	169.995	21.329	4.42	440.786	356.214	44.694	47.723
764	**169.818**	**22.227**	**4.29**	**426.831**	**337.169**	**44.132**	**50.366**
711	119.136	16.756	4.16	413.292	297.708	41.872	40.018

The obtained values of motor efficiencies in accord but the pump efficiency is showing a higher value. Figure 3.3 shows comparative analysis between both our experimental work and work of Gupta and Goel [1].

The leakage is still there as evident from repeated priming being required for the pump. On comparison with Experiment 1, the overall efficiency has increased but is still below 25.36% as stated by Gupta and Goel [1]. So it has been decided to purchase a new pump of same model and carry our further analysis on the new pump.

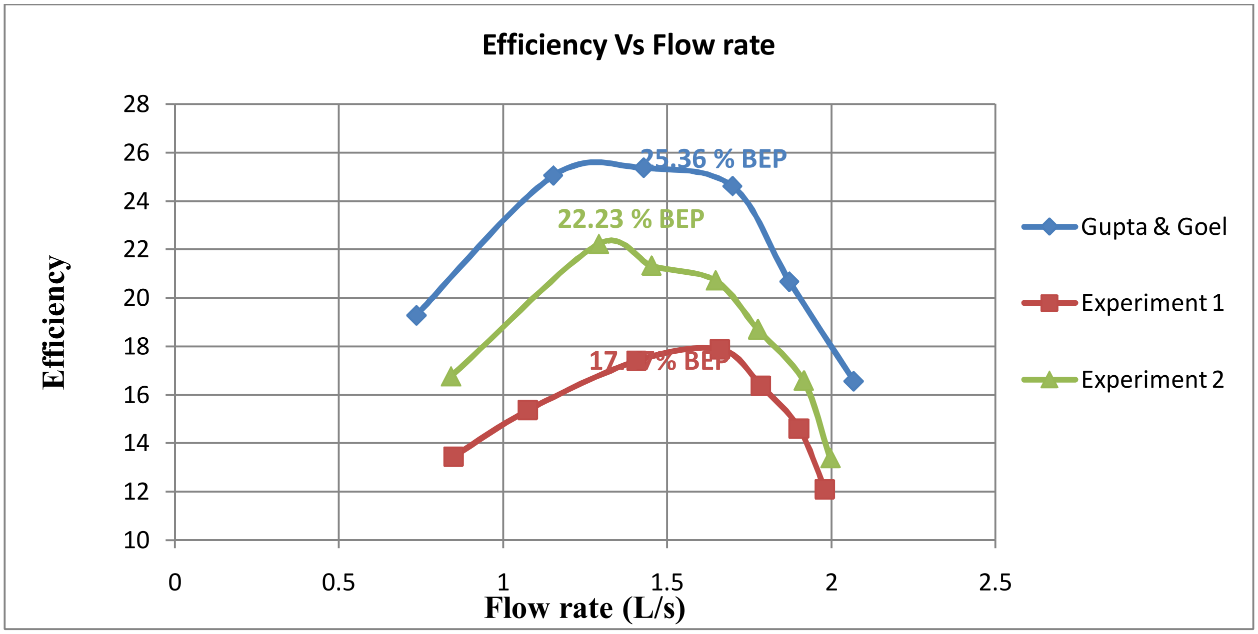

Figure 3.3 Comparisons of Obtained Efficiency Values in Experiment 1 &2 with Gupta & Goel

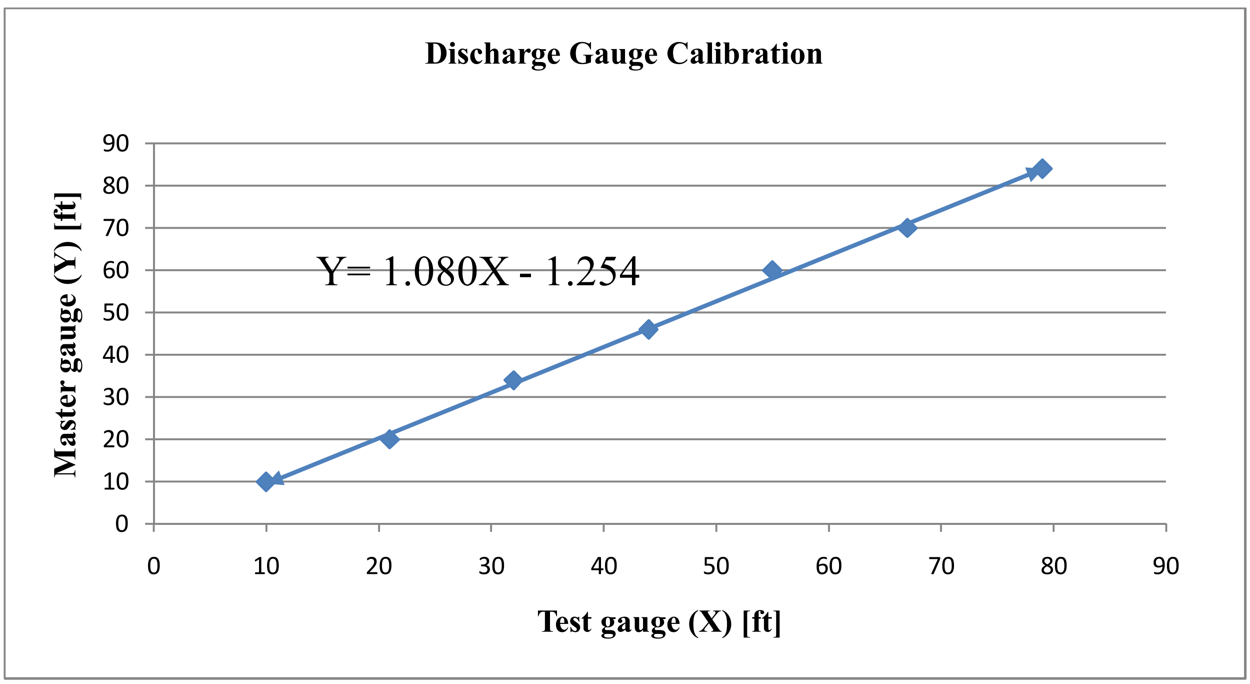

Figure 3.4 Discharge Pressure Gauge Calibration Readings

3.2 Experiments of New Crompton Greaves Pump

A new pump of the same model (Crompton Greaves MBE052) of the same rating is purchased from the market. The same procedure has been carried out in testing the new pump. But this time discharge pressure gauge was calibrated in order to get more accurate results. A master gauge was used to carry out the calibration. The calibration plot is shown on the previous page in Figure 3.4.

These calibrated values are incorporated in calculating the overall efficiency of the new pump. Table 3.7 shows efficiency values obtained from the experiment.

Table 3.7 Efficiency Calculations for new Crompton Greaves Pump

Discharge Pressure (gauge)	**Suction Pressure**		**Input Power (P_{in})**	**Flow rate (Q)**	**Efficiency (η_o)**
(atm)	**Suction Side (cm)**	**Open to atm. (cm)**	**(Watts)**	**(L/s)**	**(%)**
0.21796	70.45	25.85	832.67	2.116	15.34
0.409184	69.35	27.45	817.33	2.041	19.35
0.600408	67.55	29.15	812.25	1.941	22.43
0.791632	65.05	31.3	803.75	1.813	24.68
0.982856	63.15	33.1	791.75	1.665	26.41
1.17408	**61.15**	**34.7**	**777.75**	**1.481**	**26.96**
1.365304	59.55	36.15	742.25	1.233	26.24

At the BEP of the new pump the efficiency is 26.96% which is sufficiently close to the value of 26.56% as stated by Gupta & Goel [1]. So the pump was taken to carry out the motor test without dismantling the impeller so as to prevent any sealing problems later.

Motor test: - The setup for the motor testing was the same as used for the earlier tests. The Block Rotor Test and No-Load tests were carried out to evaluate the efficiency of the motor. The experimental readings are shown in Table 3.8 and Table 3.9.

Table 3.8 Readings from No-Load test of the new motor

S.No	Rated Voltage (V)	Current (A), I_{NL}	Input Power (W), P_{NL}
1	200	1.97	273.5

Table 3.9 Readings from Block Rotor test of the new motor

S.No	Voltage (V_{BR})	Rated Current (A), I_{BR}	Input Power (W), P_{BR}
1	56.7	4.0	197.0

Effect of Rotational Speed: - The rotational speed of the motor was also recorded in order to study its variation with the input voltage of the AC source. This was done to account for the rpm changes in efficiency evaluation, due to any voltage fluctuations which might be present during the course of the experiment. The voltage was varied using a transformer and the rpm was measured with a tachometer. Table 3.10 shows obtained rpm values.

Table 3.10 RPM Variation with Voltage

S.No	Voltage (V)	RPM
1	190	2860
2	200	2860
3	210	2880
4	220	2880
5	230	2880

It was found that rotational speed doesn't change significantly within appropriate range of voltage. Motor losses were calculated and included in the obtained values of efficiency shown in Table 3.11.

At the best overall efficiency of 26.96%, the motor efficiency of 46.15% gives a pump efficiency of 58.42%. This was much higher than 50.94% as stated by Gupta and Goel [1]. But the procedure followed by them is an approximation due to an assumption of constant power losses in the motor at all flow rates. This was assumed by them as they did not record the Current values at different flow rates. So the efficiency obtained in the current experiment with the new pump will be considered in all future references.

Table 3.11 Efficiency Calculations for the Motor and the Impeller-New Motor

Input Power (P_{in}) (Watts)	**Output Power (P_{out}) (Watts)**	**Overall Efficiency (η_o) (%)**	**Input Current (I) (Amperes)**	**Motor Power Loss (Watts)**	**Pump Input Power (P_{pump}) (Watts)**	**Motor Efficiency (η_{motor}) (%)**	**Pump Efficiency (η_{pump}) (%)**
832.667	127.719	15.338	4.145	435.632	397.034	47.682	32.168
817.333	158.126	19.347	4.035	424.664	392.670	48.043	40.269
812.250	182.218	22.434	4.010	422.212	390.038	48.019	46.718
803.750	198.369	24.680	3.980	419.290	384.460	47.833	51.597
791.750	209.063	26.405	3.945	415.909	375.841	47.470	55.625
777.750	**209.690**	**26.961**	**3.975**	**418.805**	**358.945**	**46.152**	**58.418**
742.250	194.753	26.238	3.830	405.009	337.241	45.435	57.749
689.500	160.281	23.246	3.540	378.955	310.545	45.039	51.613

Comparative Analysis: - The results of the experiment with the new pump were compared with the previously conducted experiments and the results stated by Gupta & Goel [1].

Figure 3.5, Figure 3.6 and Figure 3.7 show the plots with variation of Efficiency, Discharge Head and Suction Head versus flow rate.

Efficiency Comparisons for various flow rates are shown in Figure 3.5. Lower values of efficiency obtained in Experiment 1 and Experiment 2 can be accounted to the fact that the pump set had been disassembled earlier and its impeller used for blade profile measurements. The results from new pump set are nearly in accordance with the values obtained by Gupta & Goel [1].

Figure 3.6 compares variation in total discharge head with changing flow rates. For lower value of flow rates, discharge head values of new pump set are almost same as the ones obtained by Gupta & Goel [1].

In Figure 3.7 it can be observed that there is significant difference between total suction head for new pump set and Gupta & Goel [1] for same values of flow rates.

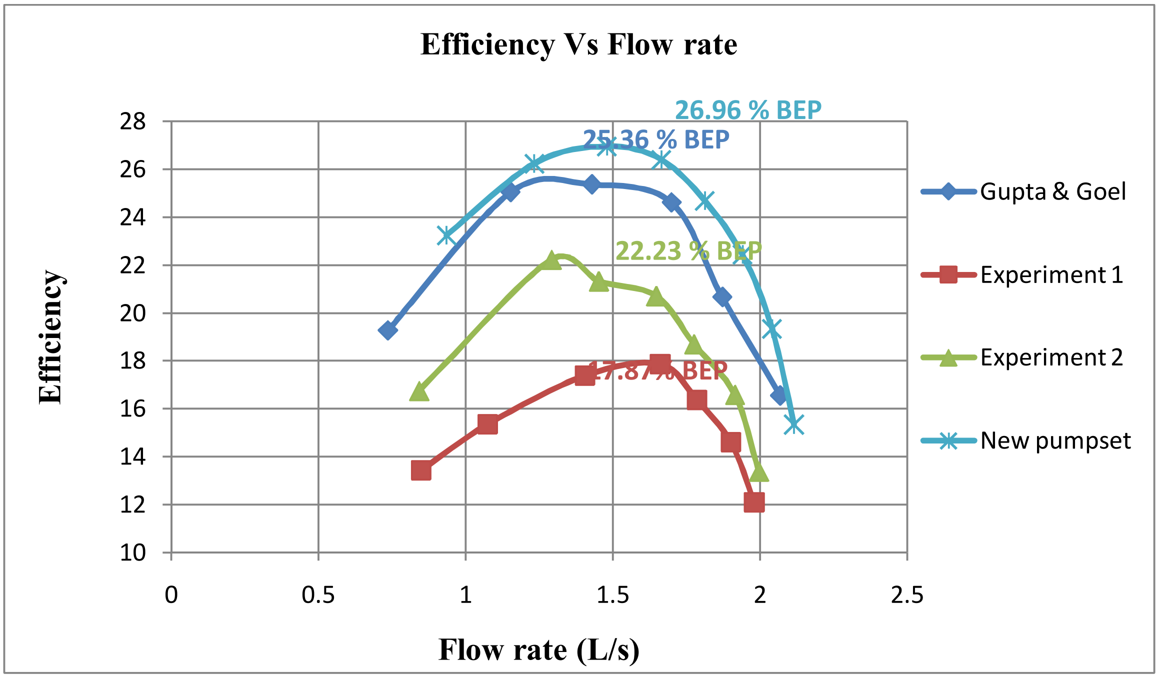

Figure 3.5 Obtained Efficiency Values in Different Experiments

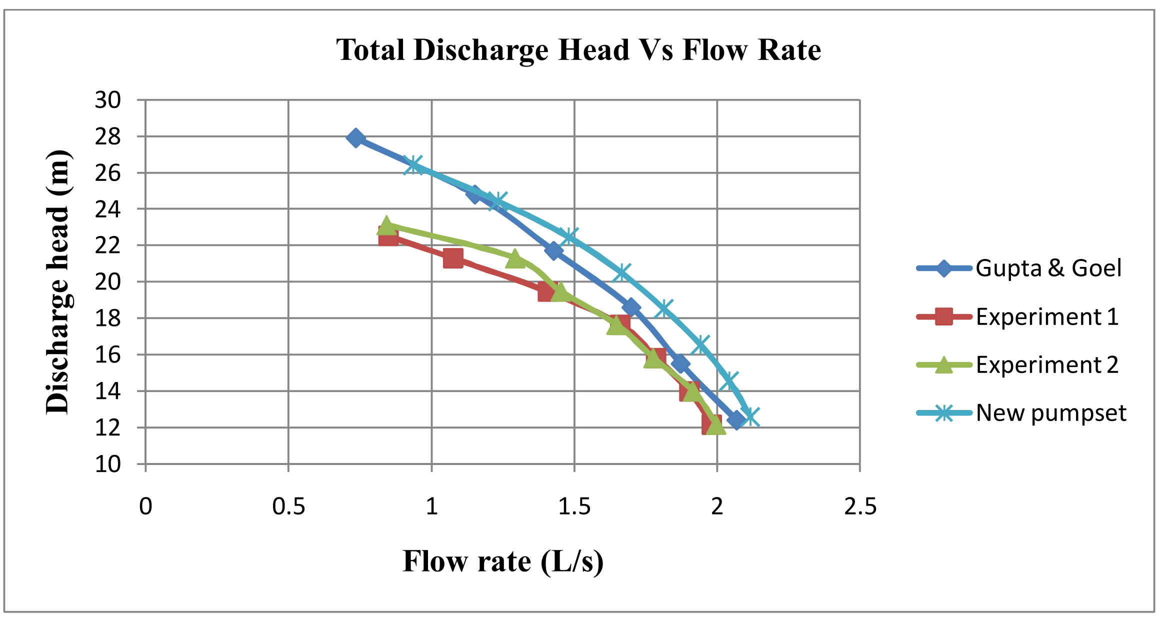

Figure 3.6 Discharge Head Variation with Flow Rate in Different Experiments

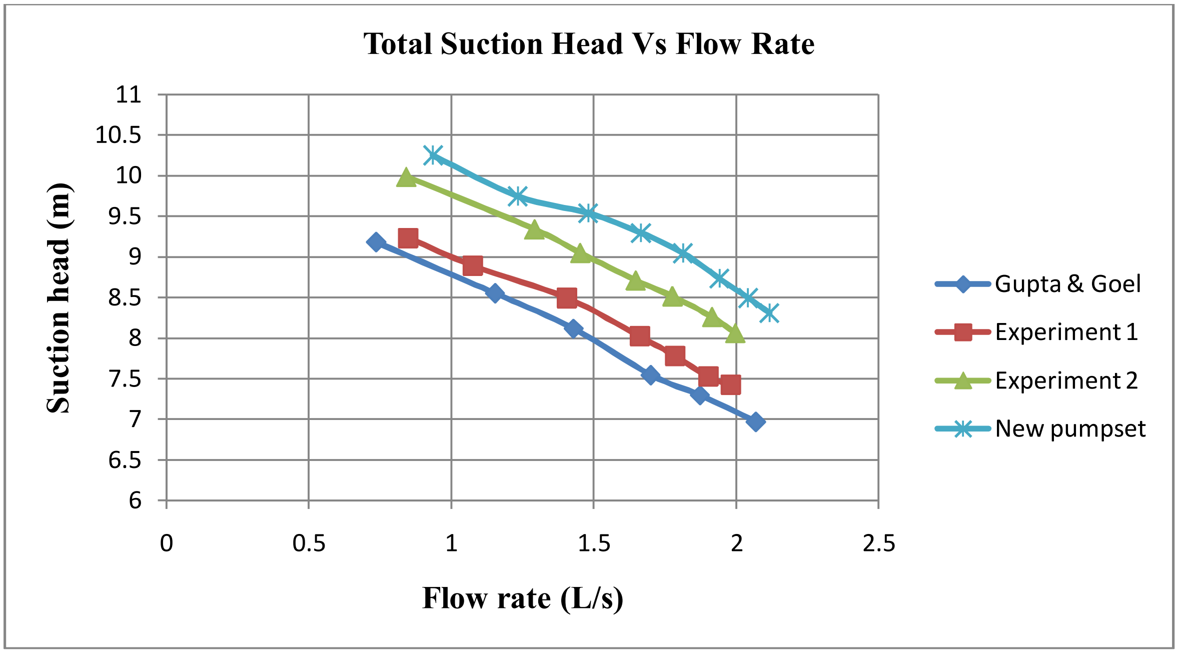

Figure 3.7 Plot of Total Suction Head Vs Flow Rate for all the experiments

3.3 Blade Profile Measurement

The impeller section was faced (Figure 3.8) from one side to make visible the blade profile of the impeller. The impeller was faced section by section from the rear side, where it gets fixed onto the motor shaft, on the lathe in the machine shop. It was machined precisely up to the section where the flow volume begins. Proper care was taken so that the blade profile doesn't get damaged during the facing process.

Figure 3.8 Facing of the impeller on machine lathe

Coordinate Measuring Machine (CMM) (Figure 3.9) was used for measuring the profile of the impeller. A number of points were taken along the length of the all the three blades. The probe was made to touch the blade's lateral surface and specified coordinates were noted down. The coordinates were taken of all the three blades of the impeller A, B and C.

Using MS-Excel data of blade profiles (Figure 3.10) were obtained for all three blades A, B and C. In order to obtain averaged common blade profile, all points of blades B and C were made to rotate such that they get superimposed (Figure 3.11) on blade A. This was done in order to take care of manufacturing or other errors in the individual blade profiles. Also, this increases the number of data points available for getting blade profile. We have used curve fitting to obtain the blade profile.

Figure 3.9 Impeller under CMM

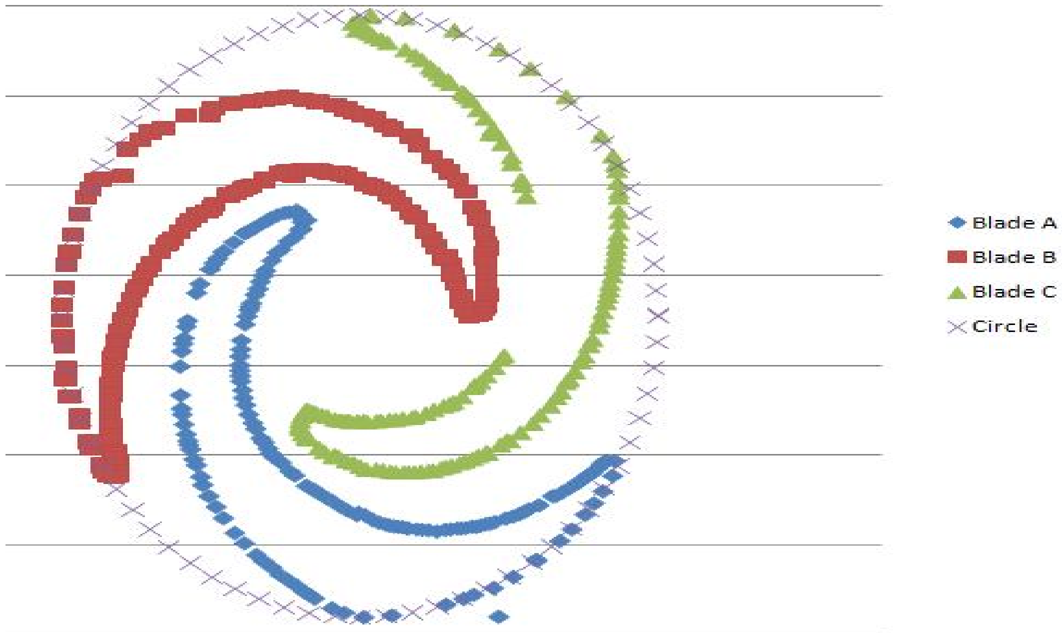

Figure 3.10 Blade Coordinates measured using CMM plotted in MS-Excel

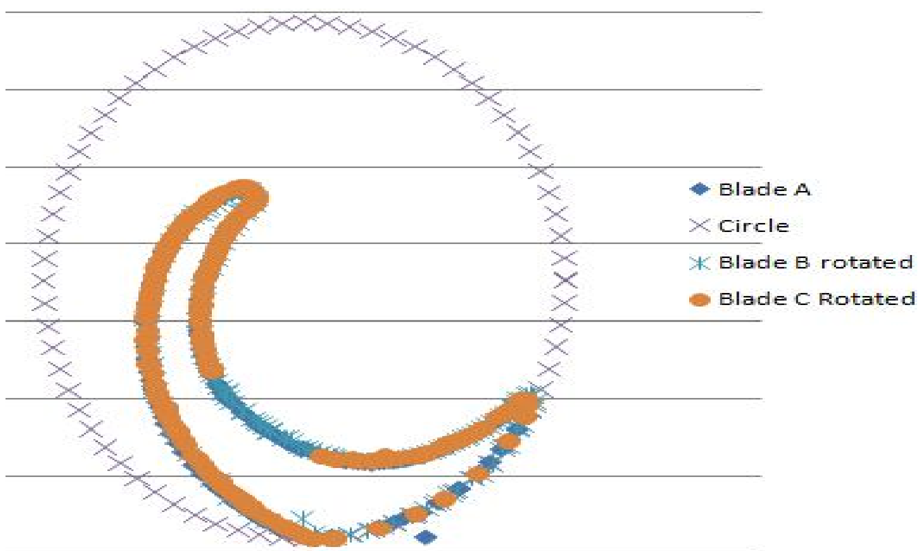

Figure 3.11 Superimposed Data Points of all the three blades

These superimposed points were plotted in MATLAB and the Curve Fitting Tool (CFT) was used. The method of linear least squares was employed to obtain the best fit curve for both the concave and convex sides of the blade. Different arrays were made for each case and the scatter plot of the superimposed points was first plotted for both the convex and concave sides of the blade. Since the number of points on the concave side is large, the curve was broken into two approximate halves to improve the goodness of the fit and minimize the residuals. A polynomial type of fit of 4th degree with no robustness is incorporated. Figure 3.12, Figure 3.13 and Figure 3.14 shows the images and equations of the curves fitted.

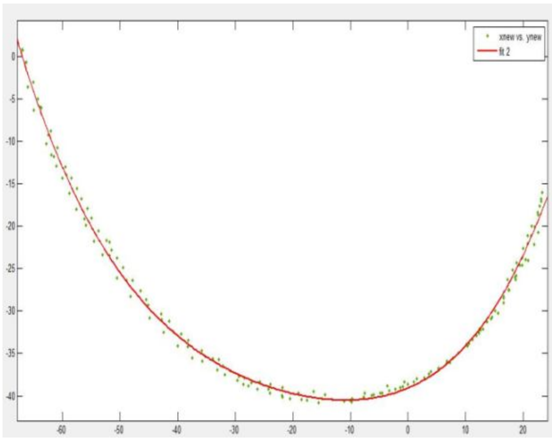

Linear model Poly4:

$f(y) = p1*y^4 + p2*y^3 + p3*y^2 + p4*y + p5$

Coefficients :

p1 = 3.405e-006
p2 = 0.0002934
p3 = 0.01743
p4 = 0.2917
p5 = -39.07

Goodness of fit:
SSE: 112.2
R-square: 0.9938
Adjusted R-square: 0.9937
RMSE: 0.848

Figure 3.12 Curves Fitting on the Convex Side

As already stated, the concave side of the blade is split into two halves; y < -30 and y > -30

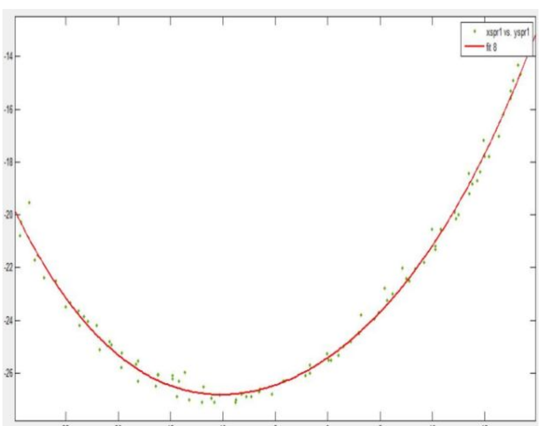

Linear model Poly4:

$f(y) = p1*y^4 + p2*y^3 + p3*y^2 + p4*y + p5$

Coefficients (with 95% confidence bounds):

p1 = 4.608e-006
p2 = 8.305e-005
p3 = 0.0138
p4 = 0.2743
p5 = -25.42

Goodness of fit:
SSE: 10.24
R-square: 0.9914
Adjusted R-square: 0.991
RMSE: 0.3431

Figure 3.13 Curve fitting on the concave side (for y > -30)

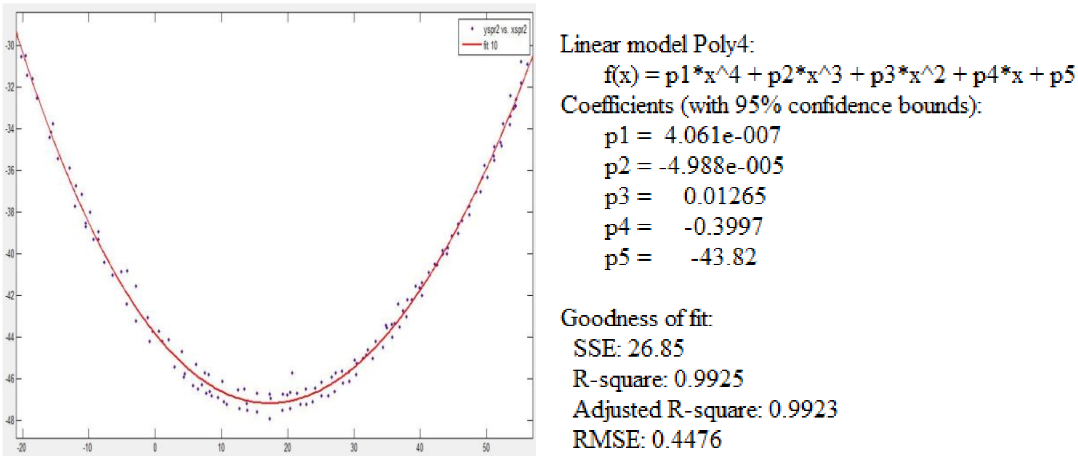

Figure 3.14 Curve fitting on the concave side (for y < -30)

3.4 CAD Modeling

The equations of the curves generated by the Curve Fitting Tool (CFT) of MATLAB that fits the best curve on the least square regression basis are obtained. The convex side of the blade profile is generated by fitting a single curve through all the measured data points while the concave side is broken into two halves. Through the known equations, a number of points were generated in MS Excel such that the curve directly gets imported in SolidWorks'08. Then both the curve profiles were linked and the final blade profile was generated. Then a circular pattern of 3 such profiles was created to complete all the blades of the impeller and the solid model is generated according to the dimensions (Figure 3.15).

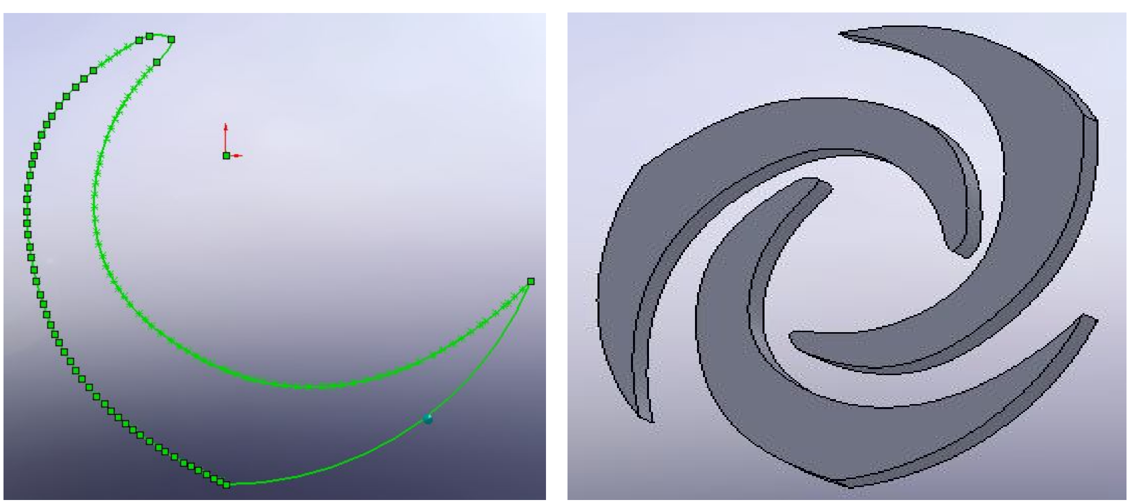

Figure 3.15 a) Blade profile with both the curves b) Circular array of three blades

Then the inlet and outlet passages were also modeled with appropriate dimensions. The model of the impeller was created and is as shown in Figure 3.16.

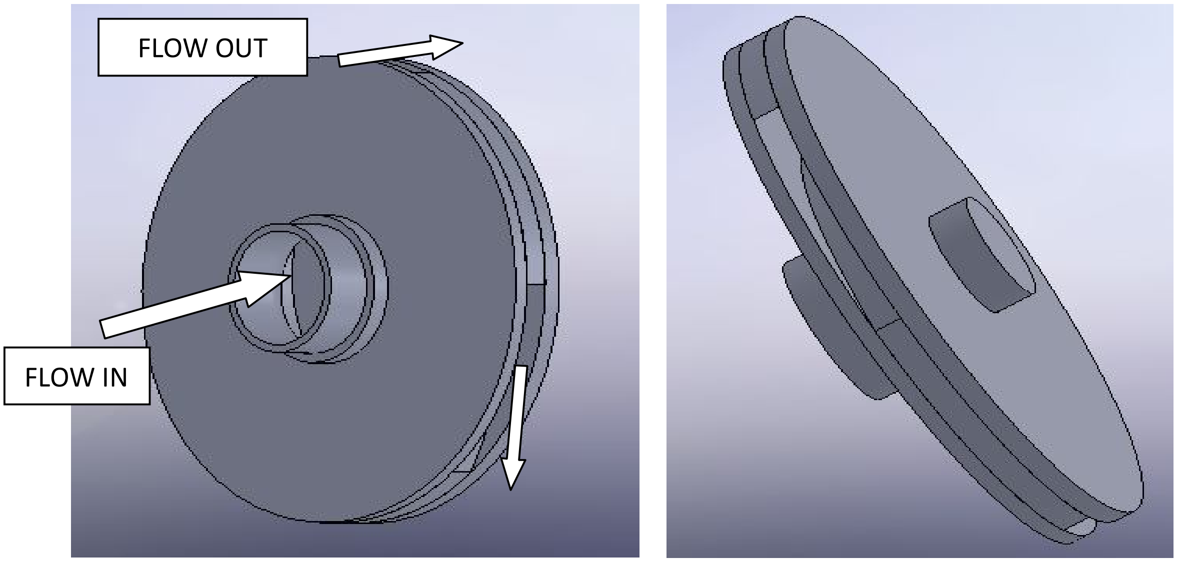

Figure 3.16 Different views of the impeller showing the flow directions

In order to carry out the simulation and analyze the flow characteristics, it is the fluid flow volume within the impeller that is required. So a solid body of same outer dimensions as that of the impeller was first created. The overlapping part of the impeller with the solid body was subtracted using the **Combine** feature in Solid Works in order to obtain the flow volume (Figure 3.17).

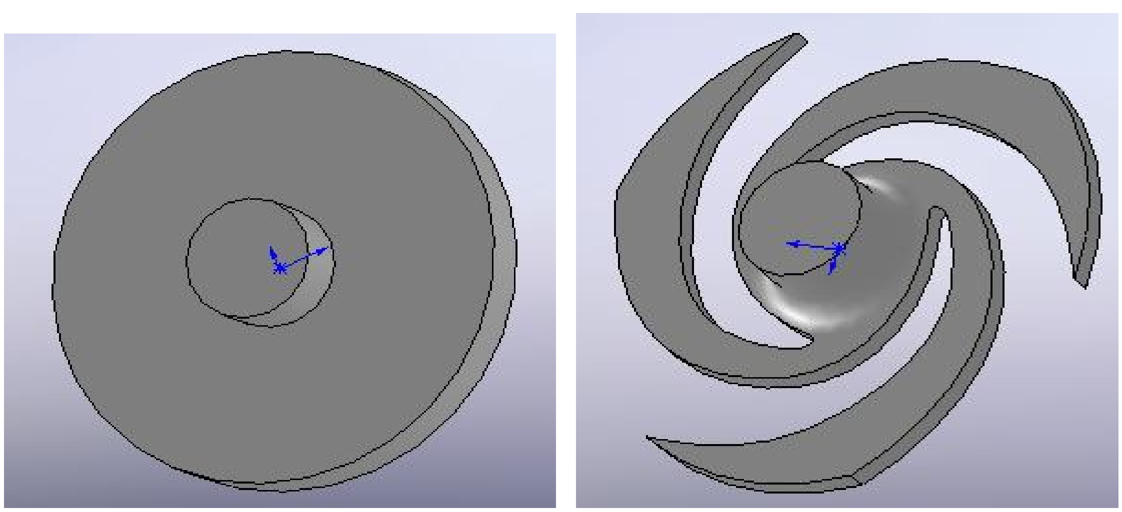

Figure 3.17 a) Solid body with same outer dimensions b) Flow volume inside the impeller

It is this flow volume that is exported to GAMBIT for meshing and then to FLUENT for running the flow simulation with appropriate boundary conditions.

3.5 Experiments using RPT Impeller

The CAD model of the existing impeller is made and subsequently fabricated using Rapid Prototyping technique. The aim is to decrease roughness values by changing to a different manufacturing process (RPT using Poly-Amide 2200 in this case) instead of cast iron. Then the impeller is mounted on the already disassembled motor shaft and the casing is sealed. In order to test the performance of this pump the experiment is carried in the same way as mentioned in the previous report. The experimental efficiency values are tabulated below in Table 3.12.

It can be seen that the maximum efficiency that could be obtained is 9.56% as compared to 22.23% obtained using the old impeller. The drastic drop in the overall efficiency could be either due to damage of the impeller or improper assembly. When the casing is opened, it is observed that there is translational motion of the impeller on the motor shaft and this causes misalignment of the impeller outlet and the centre of the volute. Hence there is drop in the efficiency. Then the experiment is repeated using a washer to hold the impeller in the correct position rigidly and to prevent any arbitrary motion of the impeller. Sufficient care is taken in the assembly and the sealing of the pump. Then the experiment is repeated again according to the Indian Standards. The experimental values are shown in Table 3.13.

TABLE 3.12 Efficiency calculations with PA2200 Impeller-Experiment 1

Discharge Pressure (gauge)	**Suction Pressure**		**Input Power (P_{in})**	**Flow rate (Q)**	**Efficiency (η_o)**
(atm)	**Suction Side (cm)**	**Open to atm. (cm)**	**(Watts)**	**(L/s)**	**(%)**
0.090477	63.7	32.3	955	1.521	5.62
0.281701	62.5	33.4	972	1.441	7.82
0.472925	61.9	34.2	1079	1.311	8.59

0.664149	**61**	**35**	**1147.5**	**1.238**	**9.56**
0.855373	59.6	35.9	1229.5	1.084	9.34
1.046597	56.5	39	1146	0.867	9.11

TABLE 3.13 Efficiency calculations with PA2200 impeller-Experiment 2

Discharge Pressure (gauge)	**Suction Pressure**		**Input Power (P_{in})**	**Flow rate (Q)**	**Efficiency (η_o)**
(atm)	**Suction Side (cm)**	**Open to atm. (cm)**	**(Watts)**	**(L/s)**	**(%)**
0.090477	62.7	31.5	896	1.537	6.05
0.281701	61.2	32.5	904	1.443	8.38
0.472925	60.3	33.6	879	1.358	10.84
0.664149	61.4	33.2	874	1.301	13.45
0.855373	60.6	35.3	873.7	1.235	15.20
1.046597	59.6	36.2	869	1.179	17.02
1.237821	**58.9**	**37.1**	**869.9**	**1.067**	**17.58**
1.365304	57.8	38.2	1050	0.992	14.60

It can be seen that there is an improvement in the efficiency as compared to Experiment 1 but it still falls below the value of 22.23% obtained using the original CI impeller. The head has also increased. The cause for the low efficiency is still uncertain even though the material used has a low surface roughness. It has been decided to check whether the performance of the motor has changed.

Motor test: - The experimental readings are shown in Table 3.14 and Table 3.15. Table 3.16 depicts individual motor and pump efficiency calculations.

Table 3.14 Readings from No-Load test of the new motor

S.No	Rated Voltage (V)	Current (A), I_{NL}	Input Power (W), P_{NL}
1	200	2.57	306.5

Table 3.15 Readings from Block Rotor test of the new motor

S.No	Voltage (V_{BR})	Rated Current (A), I_{BR}	Input Power (W), P_{BR}
1	54.4	4.0	190.0

Table 3.16 Efficiency Calculations for the Motor-Impeller-PA 2200 Experiment 2

Input Power (P_{in}) (Watts)	Output Power (P_{out}) (Watts)	Overall Efficiency (η_o) (%)	Input Current (I) (Amperes)	Motor Power Loss (Watts)	Pump Input Power (P_{pump}) (Watts)	Motor Efficiency (η_{motor}) (%)	Pump Efficiency (η_{pump}) (%)
896	54.125	6.04	4.145	4.81	393.1588125	43.879	13.767
904	75.710	8.38	4.035	4.78	404.57525	44.754	18.713
879	95.212	10.83	4.010	4.56	403.976	45.959	23.569
874	117.423	13.44	3.980	4.49	406.4988125	46.510	28.886
873.7	132.688	15.19	3.945	4.55	399.7578125	45.755	33.192
869	147.754	17.00	**3.975**	4.53	397.2143125	45.709	37.198
869.9	**152.742**	**17.56**	**3.830**	**4.61**	**389.4313125**	**44.767**	**39.222**
1050	153.098	14.58	3.540	4.66	564.02725	53.717	27.144

It is observed that there is not any significant change in motor efficiencies values but drop is clearly visible for pump efficiencies. One possible reason could be that since impeller was fabricated from RPT so there is slight change in its geometry resulting in lower flow area and thus lower pump efficiencies.

3.5 Experiments using modified RPT Impeller

Another RPT Impeller was fabricated by taking into account above anomalies. Again all pump performance parameters are evaluated by carrying out designed set of experiments. In order to check coherence of results, experiments were conducted thrice. The experimental values are shown in Table 3.17, 3.18 and 3.19.

Table 3.17 Efficiency calculations with Modified PA2200 impeller-Experiment 1

Discharge Pressure (gauge)	**Suction Pressure**		**Input Power (P_{in})**	**Flow rate (Q)**	**Efficiency (η_o)**
(atm)	**Suction Side (cm)**	**Open to atm. (cm)**	**(Watts)**	**(L/s)**	**(%)**
0.090477	64.7	31.8	1000	1.663	6.15
0.281701	63.6	32.7	1020	1.560	8.34
0.472925	62.8	33.5	1024	1.464	10.35
0.664149	62.2	34.1	1010	1.405	12.62
0.855373	61.2	34.8	1008	1.334	14.38
1.046597	**60.6**	**35.7**	**997**	**1.273**	**16.19**
1.237821	59	36.9	985	1.078	15.72
1.429045	56.3	39.3	957	0.930	15.47

Table 3.18 Efficiency calculations with Modified PA2200 impeller-Experiment 2

Discharge Pressure (gauge)	**Suction Pressure**		**Input Power (P_{in})**	**Flow rate (Q)**	**Efficiency (η_o)**
(atm)	**Suction Side (cm)**	**Open to atm. (cm)**	**(Watts)**	**(L/s)**	**(%)**
0.090477	63.9	32.4	1008	1.645	5.87
0.281701	62.9	33.4	1002	1.563	8.36

0.472925	62.3	34	997.9	1.472	10.58
0.664149	61.7	34.5	1004	1.415	12.71
0.855373	61.3	34.9	1010	1.362	14.67
1.046597	**60.1**	**35.7**	**998**	**1.265**	**16.02**
1.237821	58.6	37.2	982.4	1.100	16.03
1.429045	57.3	38.4	960.2	0.937	15.65

Table 3.19 Efficiency calculations with Modified PA2200 impeller-Experiment 3

Discharge Pressure (gauge)	**Suction Pressure**		**Input Power (P_{in})**	**Flow rate (Q)**	**Efficiency (η_o)**
(atm)	**Suction Side (cm)**	**Open to atm. (cm)**	**(Watts)**	**(L/s)**	**(%)**
0.090477	64	32.4	1046	1.664	5.75
0.281701	63.1	33.3	1037	1.559	8.09
0.472925	62.4	34	1026	1.479	10.36
0.664149	61.7	34.6	1016	1.405	12.46
0.855373	61.2	35	1002	1.331	14.41
1.046597	**60.1**	**35.7**	**990.2**	**1.247**	**15.91**
1.237821	58.4	37.6	962.2	1.065	15.79
1.429045	56.8	38.9	941.2	0.905	15.35

It is observed that all the above experiments are coherent in nature with each having highest efficiencies close to 16%. Figure 3.18 and 3.19 shows how discharge head and efficiency values obtained in these experiments compares with earlier experiments. But efficiency values are still lower as compared to the 22.23% peak efficiency obtained in the case of old motor with cast iron impeller. Also discharge characteristics are showing a sharp decline from usual pump characteristics.

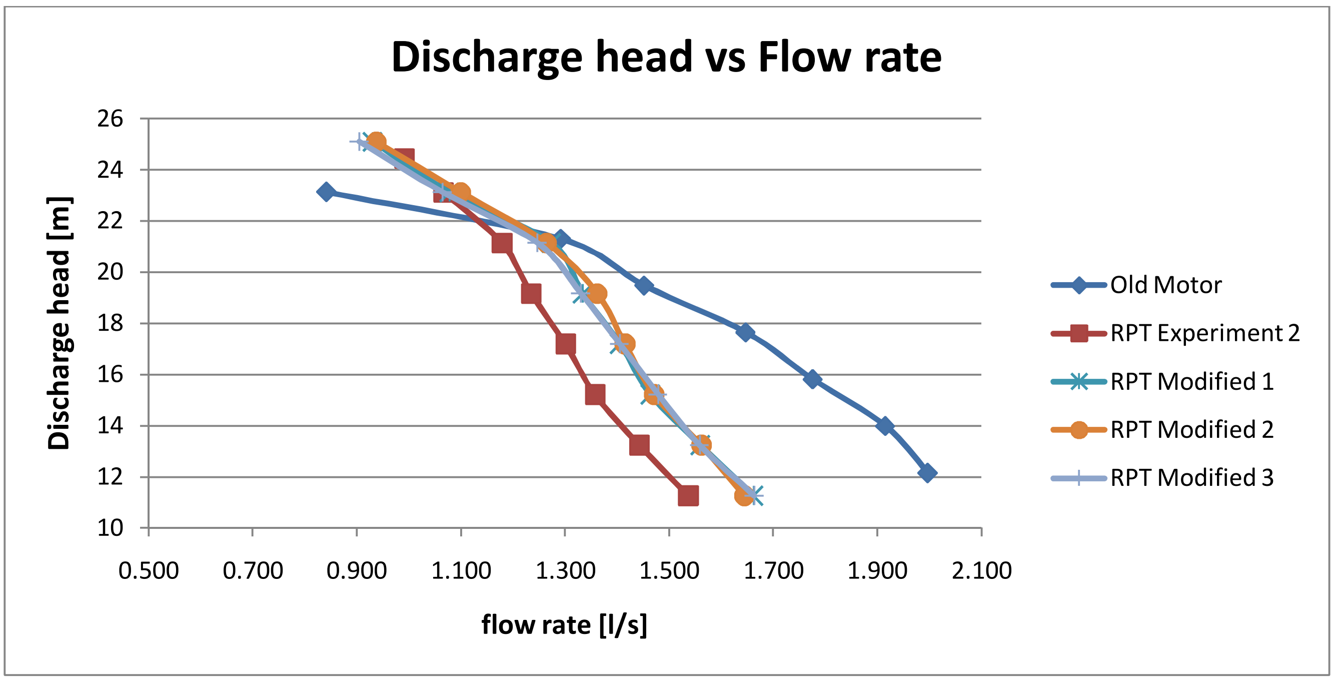

Figure 3.18 Comparison of discharge head of RPT modified experiments

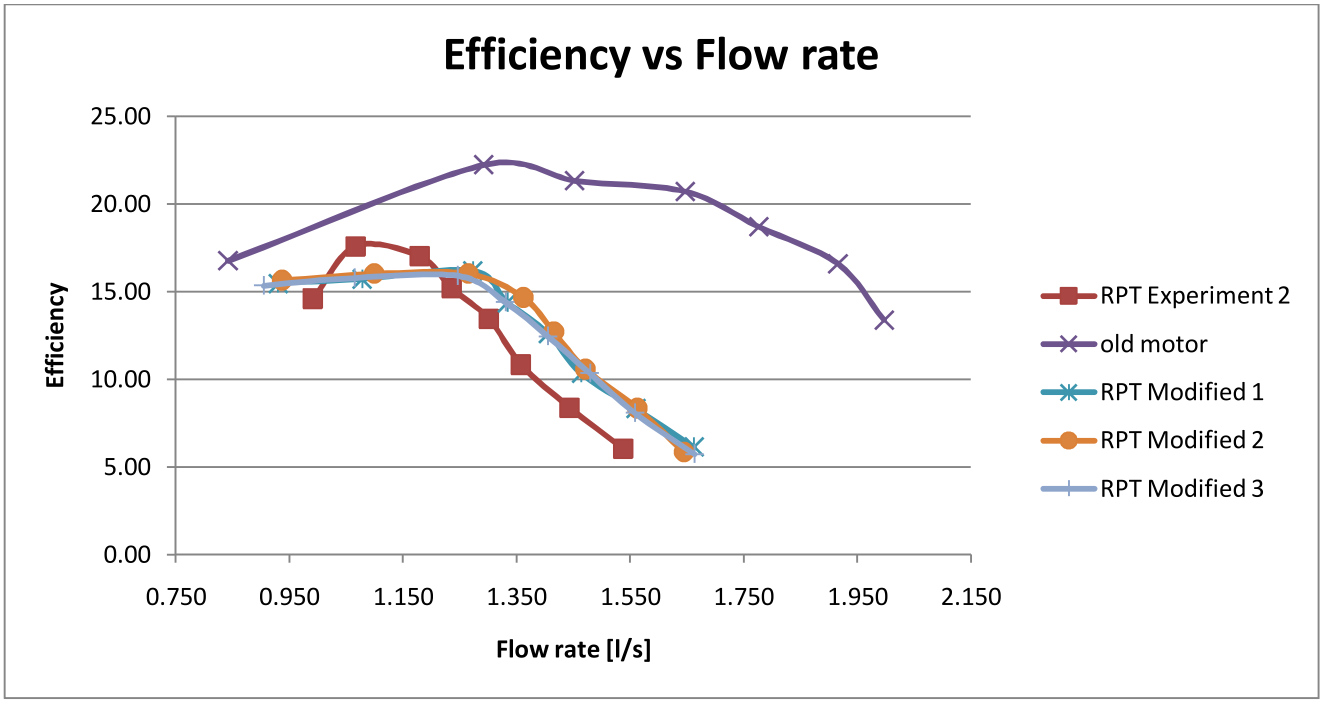

Figure 3.19 Comparison of efficiencies of RPT modified experiments

Chapter 4

Analytical and Computational Work

4.1 Meshing

In order to analyze fluid flows, flow domains are split into smaller control volumes (made up of geometric primitives like hexahedra and tetrahedra in 3D, and quadrilaterals and triangles in 2D) and discretized governing equations are solved inside each of these control volumes of the domain. The process of splitting the flow domain into smaller control volumes is called meshing. The CAD model of the impeller is directly imported into the GAMBIT software and meshed (Figure 4.1).

Meshing elements: Tetrahedral/Hybrid

Meshing Type: T Grid

4.2 Numerical Simulation

The aim of the Fluent simulation was to calculate the value of pressure rise through the impeller for a given flow rate. Flow rate at which the simulations would be carried was chosen to be the best efficiency point of the pump. The surface roughness values were taken from Gupta and Goel [1].

Impeller Flow Volume: In the simulation (Figure 4.2 and Figure 4.3) rotating frame of reference was used. This frame was given the angular velocity of impeller in the opposite sense, as though the fluid volume and the impeller were stationary and inertial frame was revolving at an angular velocity of the impeller in opposite sense. The boundary conditions used in the simulation of the impeller were:

- Uniform axial inlet velocity calculated at best efficiency point.
- Static gauge pressure at the outlet was taken to be zero.

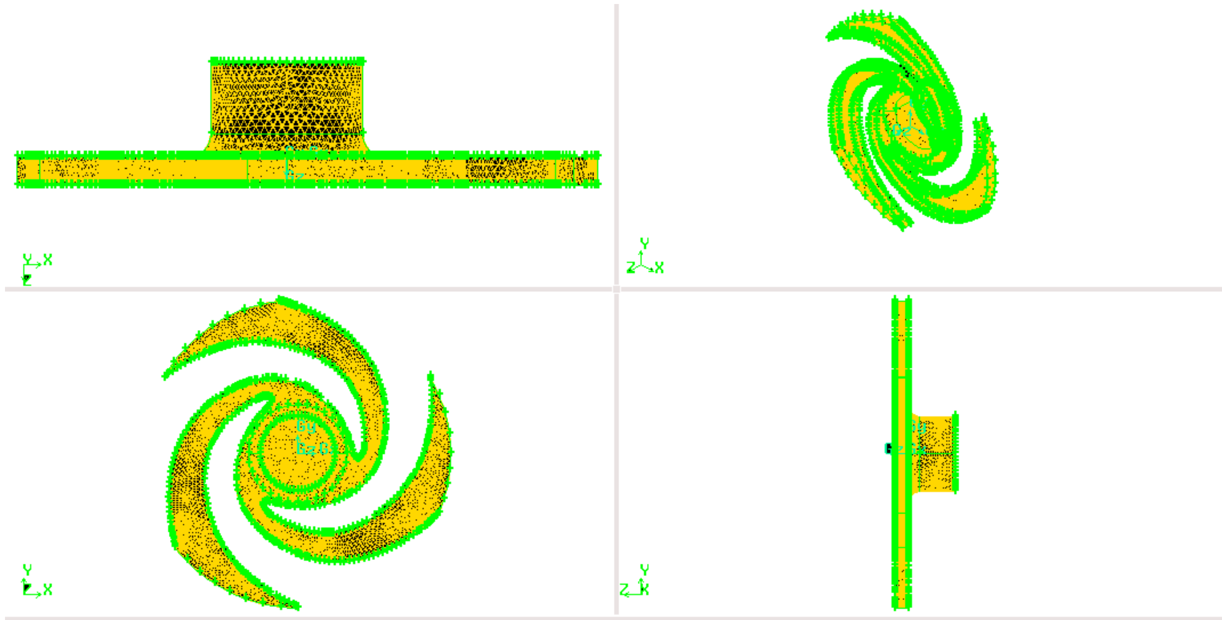

Figure 4.1 Meshed model of the flow volume in GAMBIT

The flow rate is an input for the simulation which in return gives the pressure rise as the output. Since the flow is incompressible, the absolute pressure value is not important, but pressure difference is. Since we want to find pressure rise across the impeller, we fix exit pressure arbitrarily at some value, say zero gauge and let the solver determine the inlet pressure. As such the difference gives the pressure rise.

While solving for volute, we again specify velocity/ mass flow rate at the inlet and exit pressure as zero gauge to find the pressure rise across volute in the same way.

The eye of the impeller is taken as the inlet velocity zone and the impeller exit is defined as the pressure outlet zone. We determined the inlet velocity from experiments done in the Fluid Dynamics Laboratory. The best efficiency point was considered for the simulation.

- V_{inlet} = Flow rate / Suction area = 1.299 m/s
- Hydraulic diameter at the inlet = 32 mm
- Hydraulic diameter at the outlet = 37.8 mm
- Gauge pressure at the exit = 0 Pa
- Angular velocity = 293 rad/s

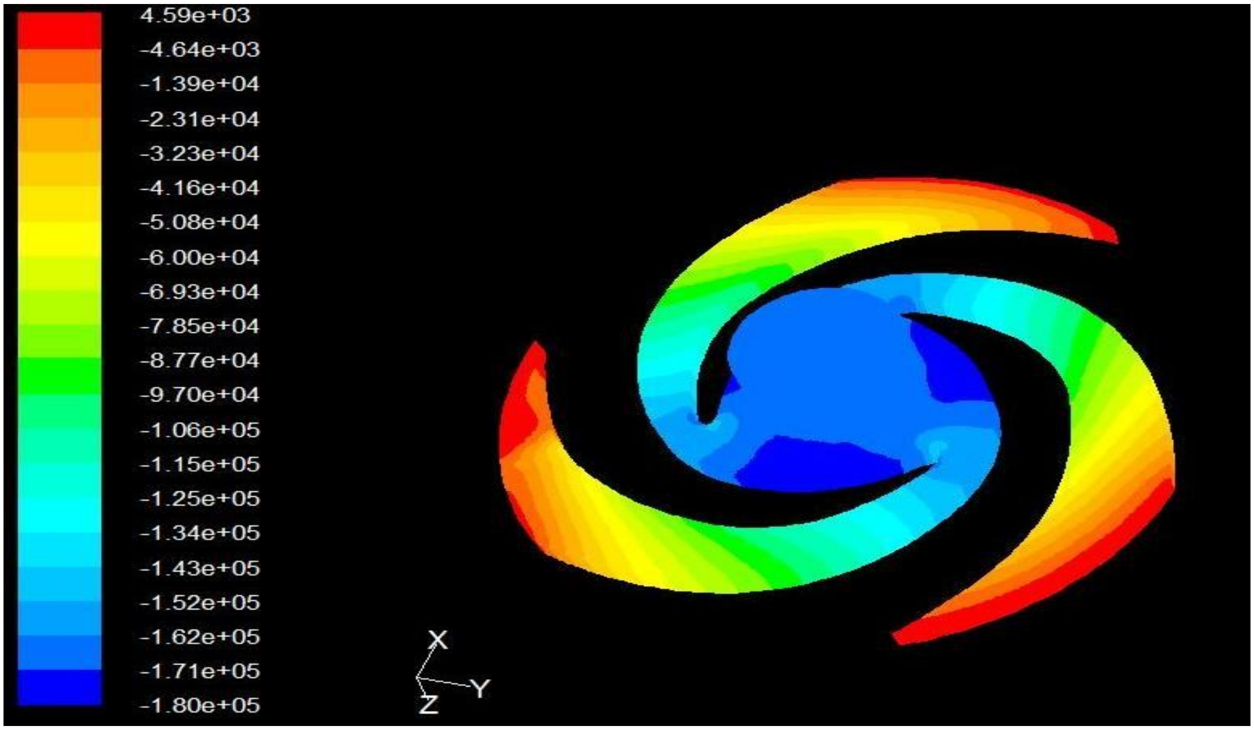

Figure 4.2 Static pressure variation in the impeller flow volume

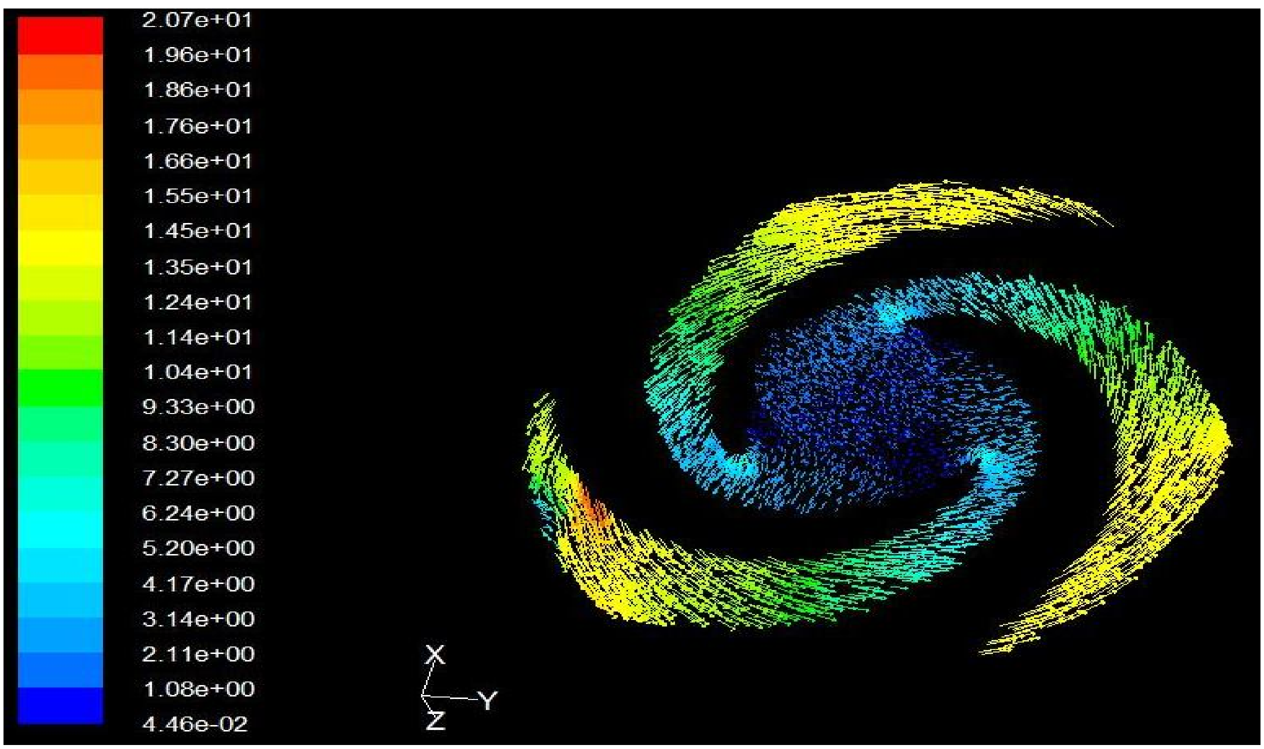

Figure 4.3 Velocity vector variation in the impeller flow volume

Results

Static pressure rise = 1.82 atm.

Velocity magnitude at the outlet = 16.7 m/s.

Radial velocity at the outlet = 1.02 m/s

Tangential velocity at the outlet = 16.67 m/s

The comparison of results with those of Gupta & Goel [1] is given in Table 4.1.

Table 4.1 Comparison of current and previous simulation results

Parameter	Current simulation	Gupta & Goel simulation
Static pressure rise [atm]	1.82	1.48
Velocity magnitude at exit [m/s]	16.7	15.37

The static pressure rise across the impeller has increased by 0.34 atm. This can be considered more accurate due to higher accuracy in measurement of blade profile.

Numerical Simulations for RPT impeller and casing

Fluent simulations are carried out for the experimentally obtained inlet velocity values using modified RPT impeller and then comparing the total heads (one obtained from the simulation and the other obtained from the experiments). This was done to compare the experimental results and the CFD results.

Modified RPT Impeller Flow Volume: - In the simulation we set up the model in the same way as mentioned for the cast iron impeller. A sample set for the BEP values is mentioned below.

- V_{inlet} = Flow rate / Suction area = 1.5448 m/s
- Hydraulic diameter at the inlet = 32 mm
- Hydraulic diameter at the outlet = 11.12 mm
- Gauge pressure at the exit = 0 Pa
- Angular velocity = 293 rad/s

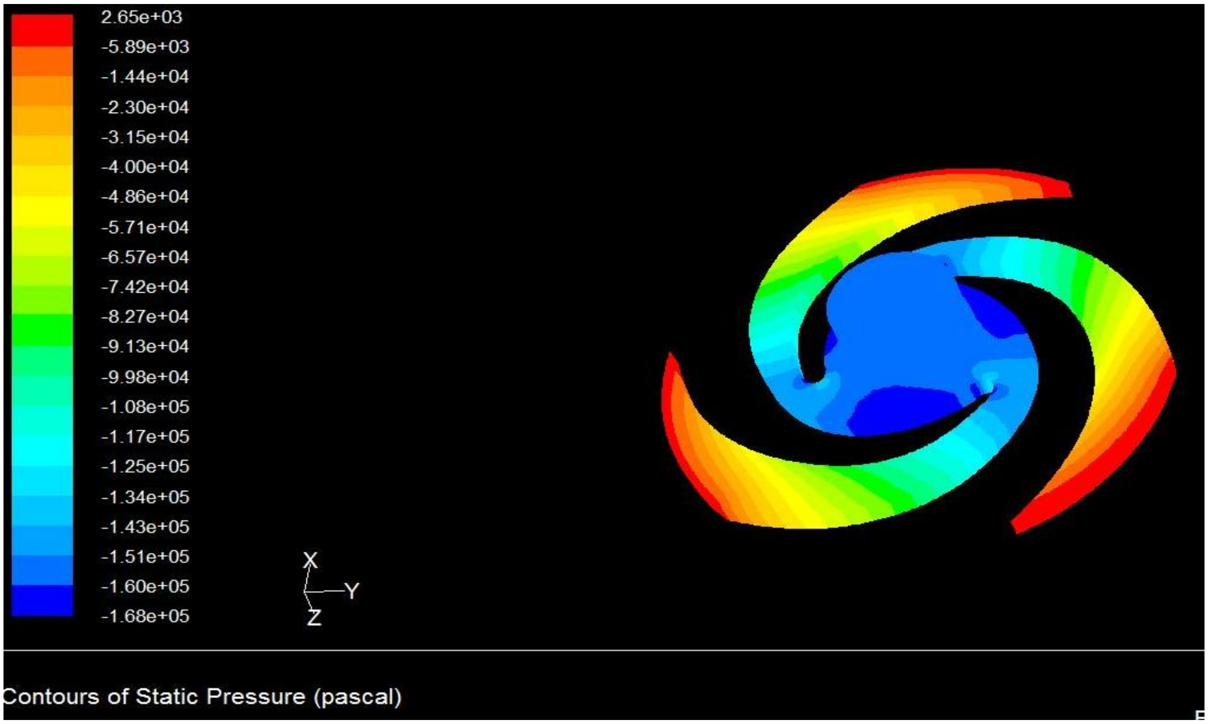

Figure 4.4 Static pressure variation in the modified impeller flow volume

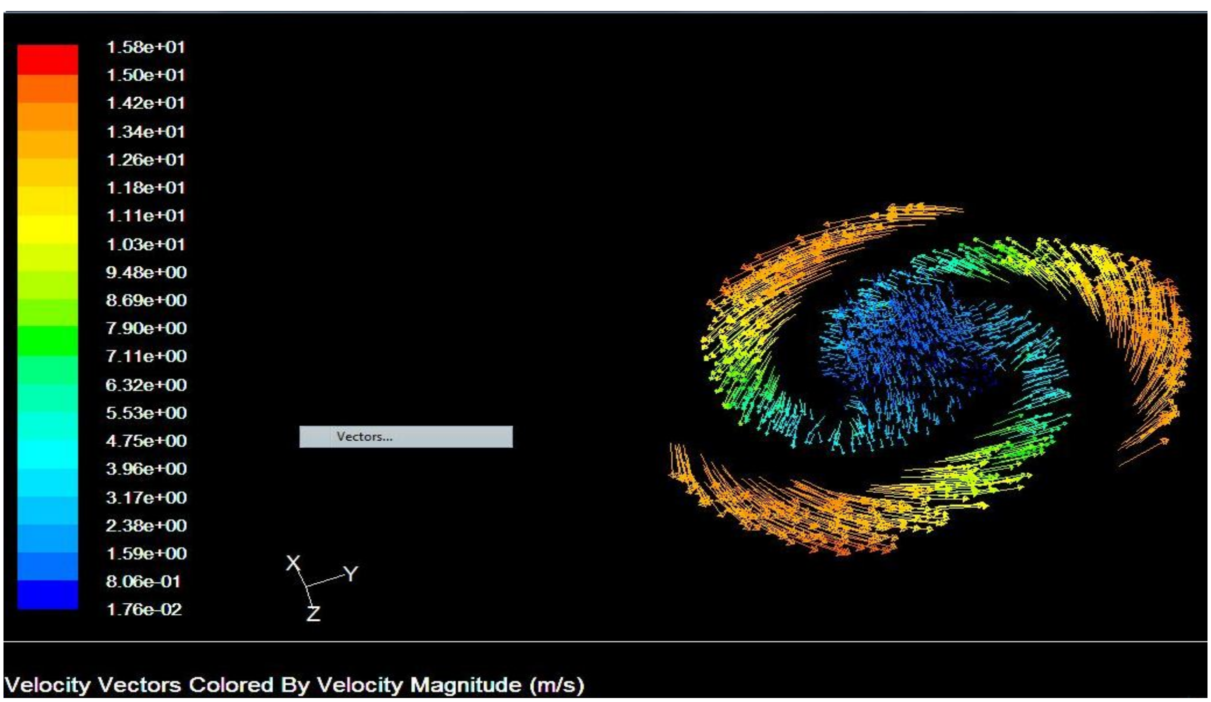

Figure 4.5 Velocity vector variations in the modified impeller flow volume

Results

Static pressure rise = 1.68 atm.

Radial velocity at the outlet = 1.186 m/s

Tangential velocity at the outlet = 13.65 m/s

Casing:

Fluent simulations for the pressure rise in the casing were carried for a whole set of experimental readings. The data obtained from the simulation of the impeller will be used as the input data for the casing.

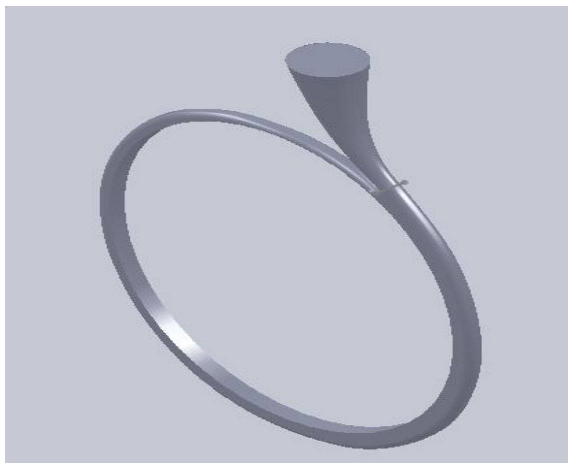

Figure 4.6: CAD model of the casing

The circumferential area where the flow exits the impeller and enters into the casing is the velocity inlet surface of the casing. The flow is taking place from the three blade passages in the impeller and these keep on moving. So we assume a uniform flow into the velocity inlet across the entire cross section of the casing circumference. For the simulation we will need the tangential and the radial velocities at the inlet of the casing.

Radial Velocity:

To calculate the radial velocity we apply continuity equation between the outlet of impeller and inlet of casing.

$V_{radimp}A_{imp}=V_{radcas}A_{cas}$

V_{radimp} is the radial velocity at impeller outlet

A_{imp} is the outlet area of impeller

V_{radcas} is the radial velocity at impeller inlet

A_{cas} is the inlet area of the casing

Now the after calculations

V_{radcas}= .45*V_{radimp}

Tangential Velocity:

To calculate the tangential velocity we need to apply the angular momentum conservation between the impeller outlet and casing inlet.

Now angular momentum at impeller exit = $\int V_{tanimp} R dm$

$$dm = V_{radimp} dA = V_{radimp} RWd\theta$$

So angular momentum $= \int_0^{2\pi} (V_{tanimp}R)V_{radimp}RWd\theta$

V_{tanimp} is the tangential velocity at impeller exit

R is radius of impeller

W is width of impeller exit

Now since the impeller has blocked area and flow passage area so the angular momentum integral for block part is zero and for the flow passage area is

Angular Momentum Integral at outlet of impeller $= \int_0^{.9\pi} (V_{tanimp}R)V_{radimp}RWd\theta$

$$= V_{tanimp} * V_{radimp}\, r^2 * .9\pi * w$$

At the inlet of casing since the flow area is the whole circumference so we get

Angular Momentum Integral at inlet of casing $= \int_0^{2\pi} (V_{tancas}R)V_{radcas}RWd\theta$

$$= V_{tancas}\, V_{radcas}\, R^2 * 2\pi * w$$

Where V_{tancas} is the tangential velocity at impeller exit

Comparing the above two we get

$$V_{tanimp} = V_{tancas}$$

A sample case for the BEP impeller data values is mentioned below:

- V_{tancas} = 13.65 m/s
- V_{radcas} = .533 m/s
- Hydraulic diameter at the inlet = 12.2 mm

- Hydraulic diameter at the outlet = 24 mm
- Gauge pressure at the exit = 0 Pa
- Angular velocity of moving inlet wall= 293 rad/s

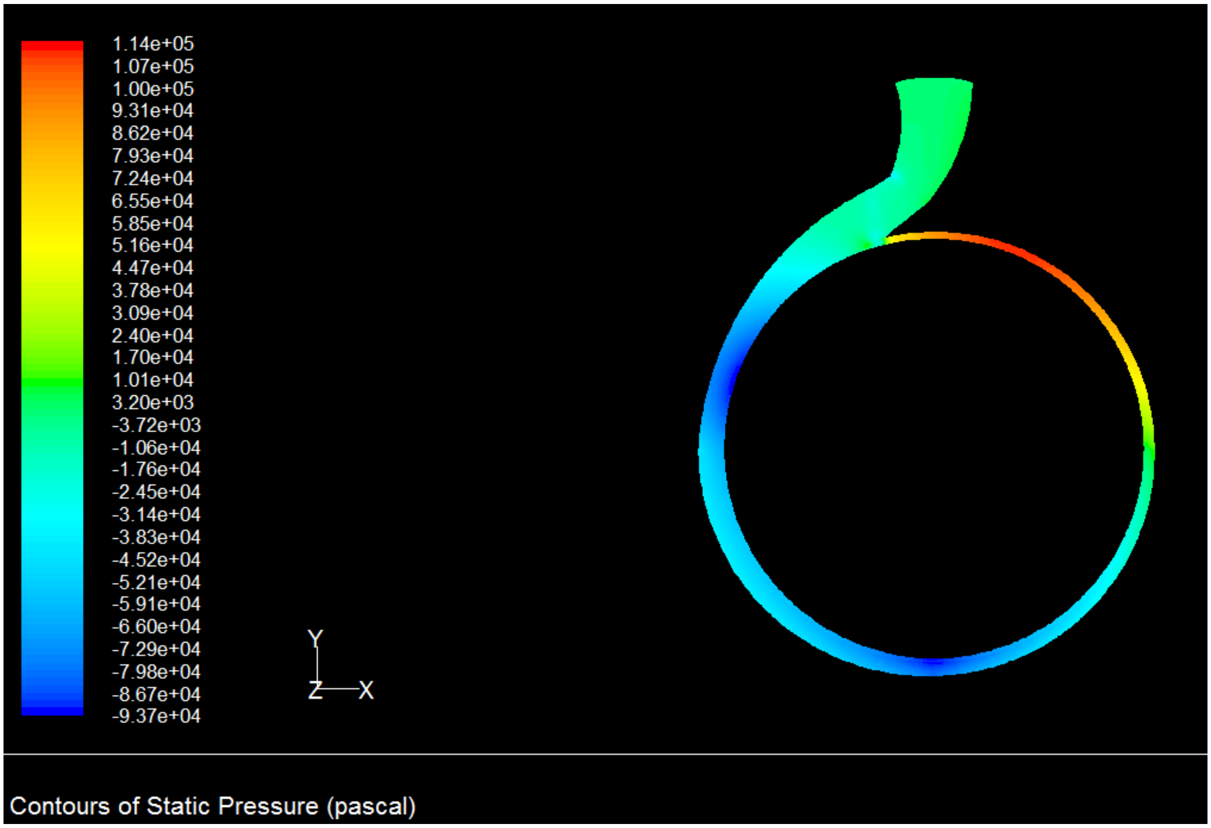

Figure 4.7: Static pressure variation in the casing flow volume

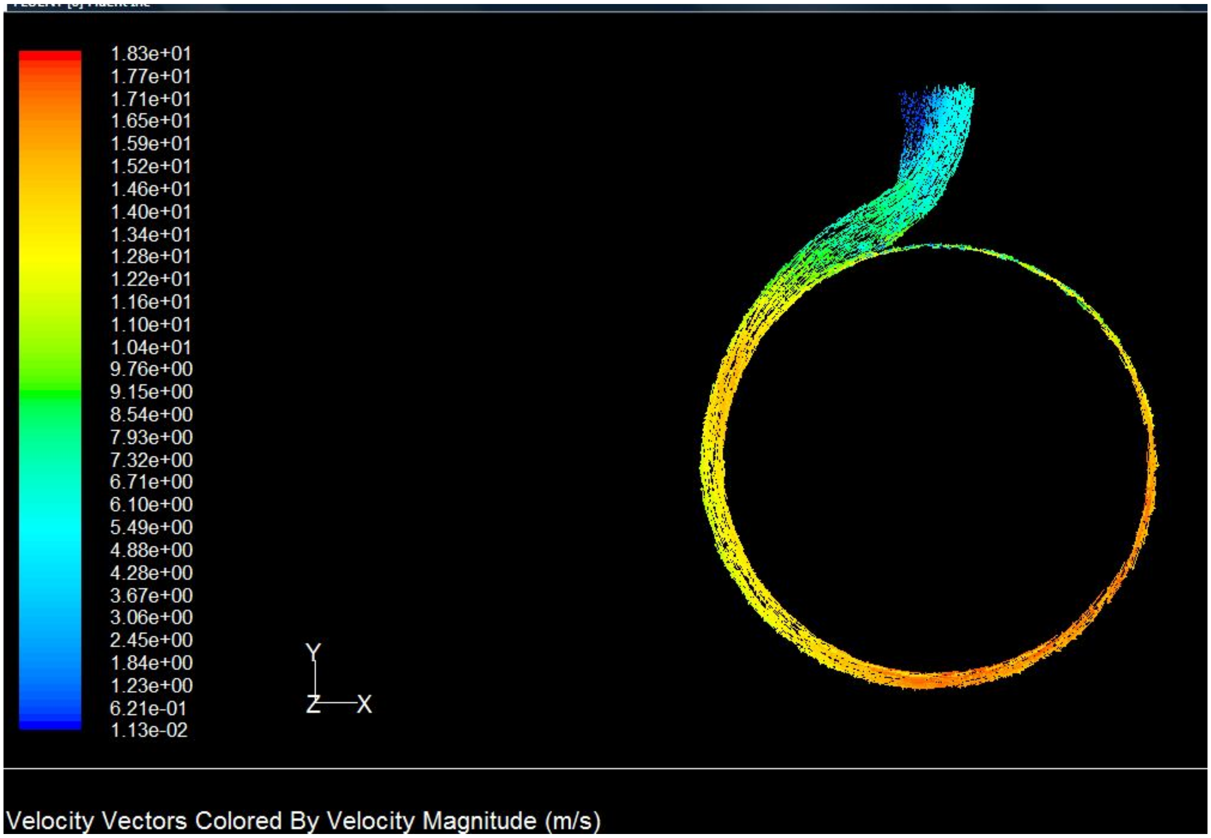

Figure 4.8 Velocity vector variation in the casing flow volume

Result:

Static pressure rise in casing = .165 atm

Velocity at exit of casing = 2.81 m/s

So now the dynamic pressure rise is

$$.5*1000*(V_{excas}^{2}-V_{inimp}^{2})$$

V_{excas} is the velocity at casing exit

V_{inimp} is the velocity at impeller inlet

So the dynamic pressure rise = .0278 atm

So the total rise pressure rise is 1.68+ .165 + .0278 = 1.873 atm

Similarly simulations for all other experimental values of flow rate were carried out. The results are in the table below:

Table 4.2: Output pressure values from simulations for experimental flow rates

Inlet Velocity (m/s)	Tangential Velocity at impeller Exit (m/s)	Radial Velocity at impeller exit (m/s)	Tangential Velocity at casing inlet (m/s)	Radial Velocity at casing inlet (m/s)	Pressure rise in impeller (atm)	Pressure rise in casing (atm)
1.77	13.12	1.38	13.12	0.62	1.81	-.645
1.71	13.34	1.32	13.34	0.59	1.77	-.02
1.62	13.41	1.17	13.41	0.53	1.72	.14
1.55(BEP)	**13.66**	**1.19**	**13.66**	**0.53**	**1.68**	**.17**
1.31	14.32	1.01	14.32	0.45	1.74	.44
1.13	8.34	0.92	8.34	0.41	1.8	-.1

From the experiments on the modified RPT impeller at the Best Efficiency Point the Total head is **12.923 m.** whereas from the simulation results we get that the Total head rise is **19.09 m.** This difference in total head rise in the simulation and experiment can be mainly due the losses in the pump.

4.3 Slip Factor: We have also determined the slip factor for the impeller. The "slippage" is due to the fact that the whole system rotating is partly solid and partly liquid in which the liquid layers are slipping over each other. We found the slip velocity V_s which is the difference between the ideal exit tangential velocity and the actual exit tangential velocity.

$V_s = V_{tangid} - V_{tangac}$

Where V_{tangid} = Ideal Tangential Velocity = Angular Velocity X Impeller Outer radius

V_{tangac} = Actual Tangential Velocity (from FLUENT CFD Analysis)

V_s = Slip Velocity

The slip velocity divided by the ideal exit tangential velocity subtracted from 1 gives us the slip factor.

Slip Factor; $S_f=[1-(V_s/V_{tangid})]$

The value for the V_s comes out to be 4.84 m/s and S_f value is .7538. While redesigning the impeller these need to be kept in mind as they are the characteristics of the impeller.

4.4 Stress Analysis using ANSYS

CAD model was used to find maximum amount of stresses that would be generated during pump operation. Pump rotational speed was taken as 2800 RPM from the pump's manufacturer data. This value was also confirmed using Tachometer while the pump was in operation. Further since we are only interested in the maximum stress that would occur, maximum pressure value was taken from CFD simulations (done in FLUENT). Maximum pressure value was 2.8 Atm (2.8e+005 Pa). Figure 4.5 and Figure 4.6 shows the stress distributions obtained for two different materials Cast Iron and PA 2200. For both of these materials Factor of Safety was calculated and is shown in Table 4.2.

Table 4.3 Impeller Stress Safety Factor

Material	Maximum Stress M (Pa)	Tensile Strength U (Pa)	Safety Factor
Cast Iron	6.24e+006	200e+006	32.05
PA 2200	5.55e+006	45e+006	8.11

Comment: For CI minimum thickness is not seemingly determined by strength consideration, but by casting consideration. Also for PA 2200 we used the same thickness as that of CI but subject to minimum allowable thickness in Rapid Prototyping.

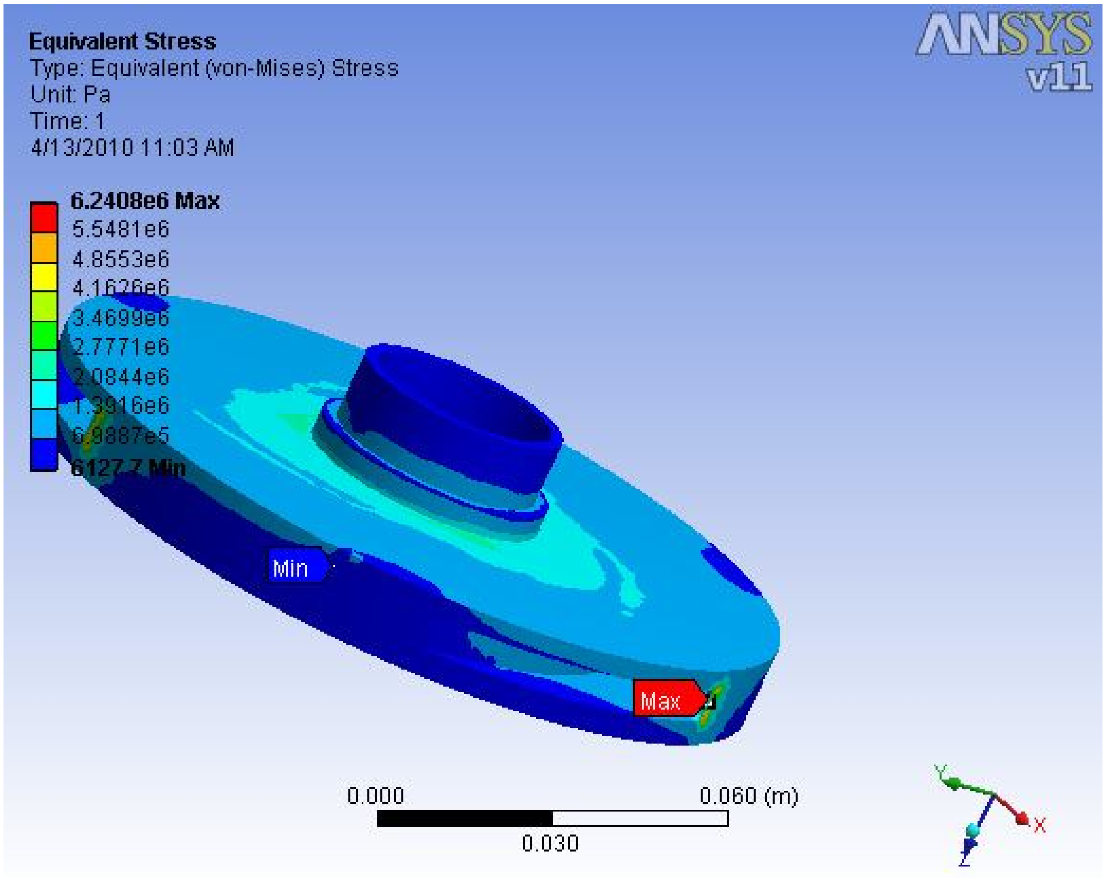

Figure 4.5 Stress Distributions for Cast Iron

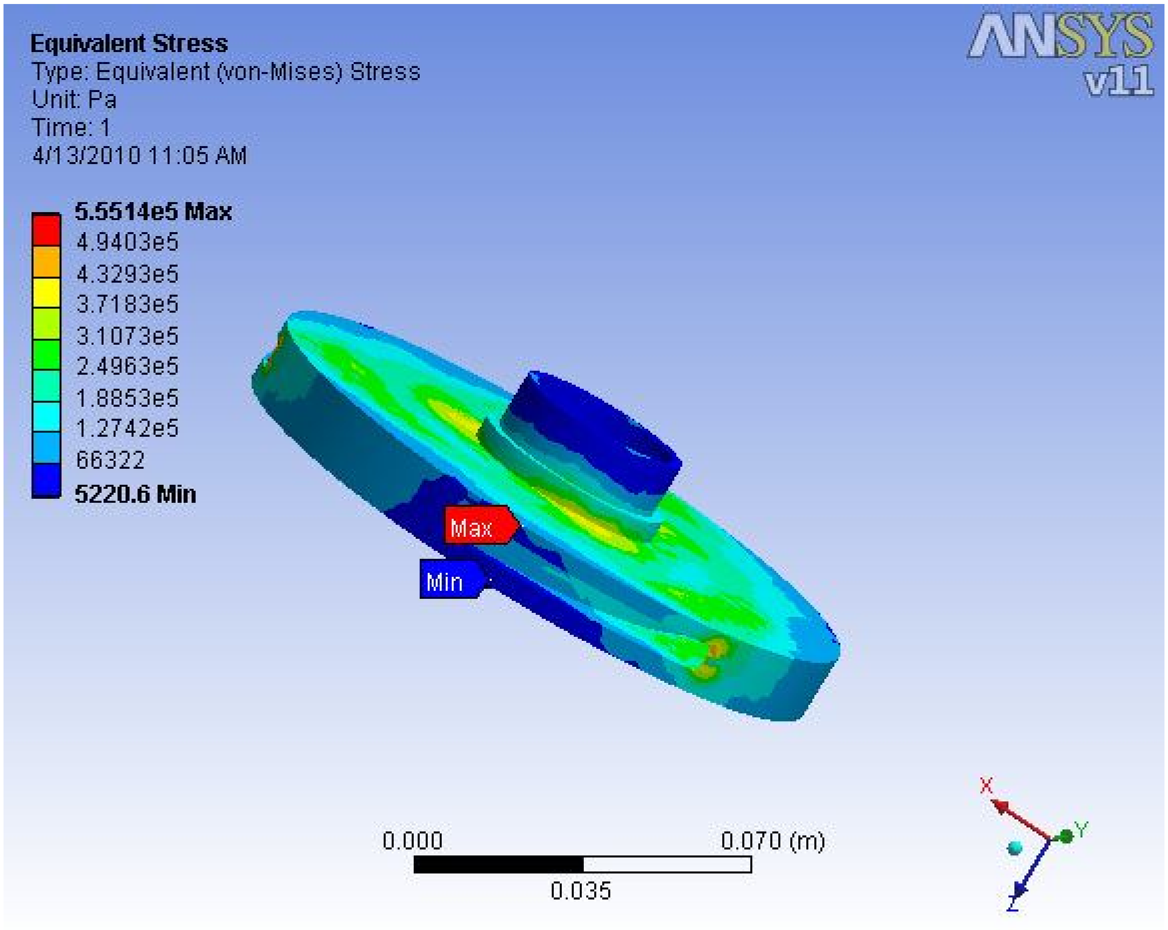

Figure 4.6 Stress Distributions for PA 2200

4.5 Half cut Impeller Fabrication using RPT

From various experiments done using RPT impeller in the old pump it was observed that their performance values are lower as compared to those obtained using cast iron impeller in the same old pump. It was concluded that the performance drop might be due to reduction in flow area as objects fabricated in RPT are subject to dimension changes due to material (PA 2200) properties. As such a half cut impeller was made using and its geometrical features were measured using CMM and then compared with the features given in the CAD model which confirmed the fact that flow area has been reduced by a small amount, thus a slight decrease in efficiency as well.

Figure 4.7: Comparison of flow volumes of CI and RPT impeller

4.6 Modified Impeller Designs

Various modifications were done in impeller designs aiming at increase in efficiency. These were done by identifying one of the parameters and then varying it to obtain various configurations.

It was decided to change the impeller blade profile from the original one obtained using the Coordinate Measuring Machine (CMM). It is to be examined that how any changes made in the curvature of the blade profile effects the losses and pressure rise in the impeller. Figure 4.7 shows the profile of a single blade of the impeller. The angle subtended by the solid blade at the centre in the original impeller is 67 degrees as shown in the figure.

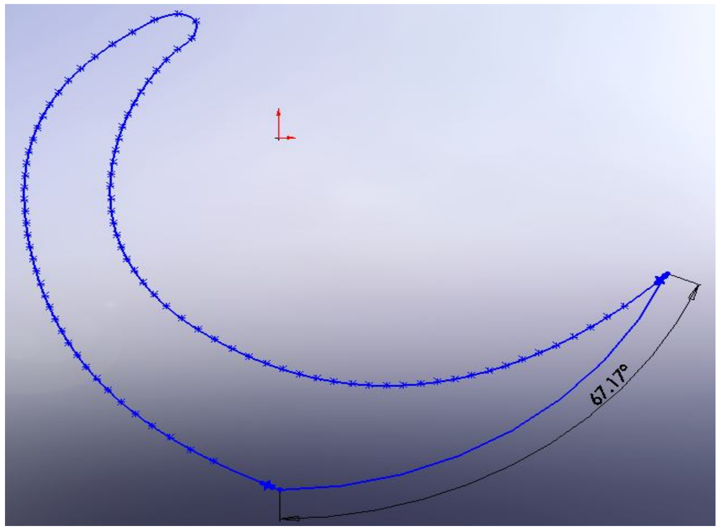

Figure 4.7 Blade Profile of Original Impeller

Both the pressure side and the suction sides are shifted in order to change the curvature and vary the angle subtended by the solid blade.

The impellers were designed using the blade profiles obtained after changing the curvature in the procedure mentioned before and their corresponding flow volumes are also generated. The CFD simulations are being carried out on these geometries in order to evaluate the effect of the change in their curvature.

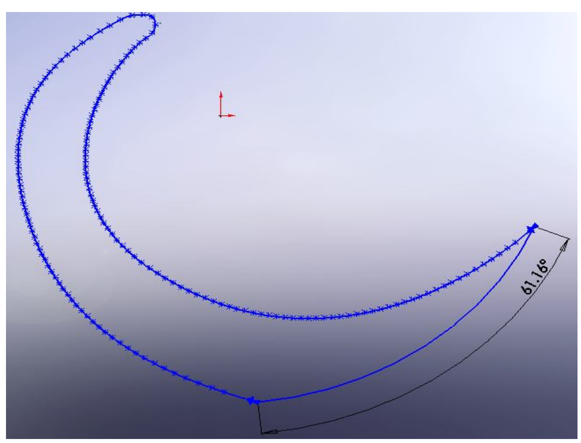

Figure 4.8 Blade Profile after shifting convex side by 6 degrees

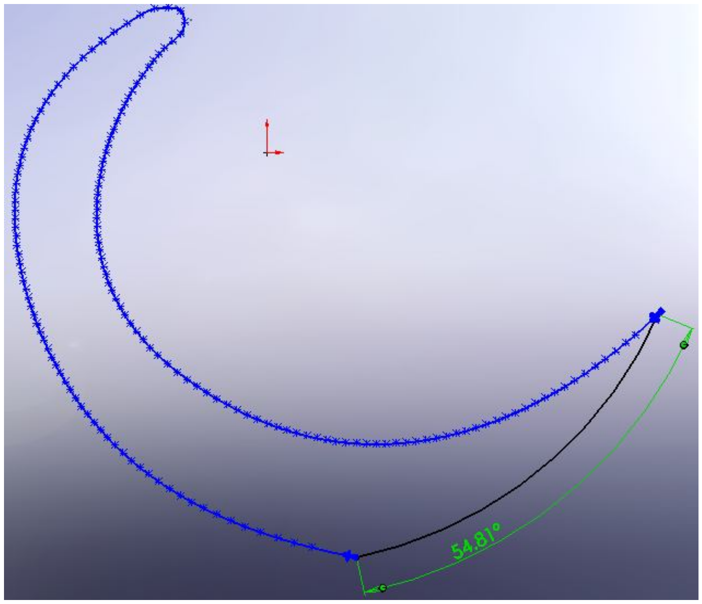

Figure 4.9 Blade Profile after shifting convex side by 12 degrees

4.7 Geometry of Casing

Earlier we were using simulation results of Gupta & Goel [1] for the casing, since using CMM it was not possible to obtain coordinate points of inner volute of casing. This problem was overcome by creating imprints of the volute profile using silicone material. This material has got unique property of setting in a very short duration of time and is elastic in nature.

Inner volute profile was measured using CMM and used for creating CAD models which were subsequently used for simulations in FLUENT & GAMBIT.

Chapter 5

Concluding Remarks

The project kicked off with the primary objective of identifying the less efficient pump and then validating the experimental results obtained by Goel and Gupta [1]. Experiments are conducted on the old motor-pump set, but the results were not in concurrence with the previous ones. Upon scrutiny it was observed that the motor resistance has increased and there are sealing problems during the assembly of the pump. So a new motor-pump set has been purchased and this new set is used in further experiments.

We were able to validate the previous experimental observations with the new set. Then in order to get the most accurate blade profile of the existing impeller, the Cast Iron impeller of the old pump set was machined from one side and the profile was measured using the Coordinate Measuring Machine (CMM). Then using SOLIDWORKS, a CAD model was designed replicating this impeller which was used in further simulations. As a first step in the redesign phase of the impeller, the material was changed to PA 2200. So the designed model was built using the Rapid Prototyping Technique (RPT). The impeller manufactured by this process has much lesser surface roughness which reduces the losses. But it came out as a surprise that there is a drastic drop in the overall efficiency. Upon examining it was observed that the impeller was free to move linearly along the length of the shaft thereby misaligning the exit of the impeller with the volute section of the casing. So a steel washer has been used to arrest the translational movement of the impeller. Still the results obtained from different experiments were not concurrent. So a new impeller was designed with an extended extrude feature on it such that the impeller stays in the correct position. The experiments conducted by this impeller obtained stable results upon repetition. But the head-flow characteristics obtained was too steeply falling and the curve is nearly linear. The flow rate has come down significantly in comparison to the CI impeller which is definitely due to some kind of leakage. But the dimensions are similar to that of the CI impeller. It was decided to check the porosity of the material by soaking a dry impeller in water and checking the difference in their weights. There was no significant change in the weight upon soaking in the impeller. Then the redesigning phase of the impeller started with shifting the curves in order to change the curvature. It was to check if there is any change in the pressure rise across the impeller due to reduction in the losses. So the geometries of the impeller were created after varying the blade profile and these geometries were used in the simulations in order to evaluate the pressure rise. This resulted in a small increment in the pressure rise across the impeller upon shifting the curve such that the angle subtended by the solid blade at the centre is reduced. This has given a hope of improving the impeller design. But the increase might also have been due to increase in the flow passage.

The simulations of the casing are previously carried out on the geometry created by Gupta and Goel. The head rise in the casing is very small as compared to the head rise in the impeller. In order to get the exact geometry of the casing we used silicone material to get the negative of the volute section. Then the variation in the depth of the volute section circumferentially is measured again using the CMM after taking a number of data points and fitting a spline curve among this point cloud.

Scope for future work

- Optimum impeller blade profile in order to get the maximum pressure rise.
- Volute can be modified in order make it more efficient.
- The roughness of the casing is also very high. So some other manufacturing process can be used in order to decrease the roughness.

Currently we are working on the optimization of the impeller blade profile. This is being done as explained in Section 4.6

References

[1] Gupta M., and Goel J., B Tech Thesis, 2008, “Experimental and Computational study of Centrifugal Pumps”, IIT Delhi.

[2] Indian Standards IS013538:1993, “Centrifugal, Mixed Flow and Axial Pumps – Code for Hydraulic Performance Tests – Precision Class”.

[3] Indian Standard IS 7572, “Guide for testing single phase AC and universal motors”.

[4] http://en.wikipedia.org/wiki/Specific_speed

[5] http://en.wikipedia.org/wiki/Computational_fluid_dynamics

[6] www.cheresources.com/centrifugalpumps2.shtml

[7] www.cheresources.com/centrifugalpumps4.shtml